Energy and Environmental Systems Group
Institute for Sustainable Energy, Environment and Economy (ISEEE)

Data Integration, Petrophysics, and Geomodelling

Wabamun Area CO_2 Sequestration Project (WASP)

Authors

Chris L. Eisinger

Jerry L. Jensen

Rev.	Date	Description	Prepared by
11	December 22, 2009	WASP Static Earth Model: Final Report	Chris Eisinger & Jerry Jensen

Table of Contents

List of Tables

List of Figures

INTRODUCTION

In order to properly assess the storage capacity, injectivity, and confinement of potential deep-saline aquifers in the Wabamun region it is critical to construct a static geological model that characterizes the Nisku aquifer with sufficient accuracy. The model, presented in this section of the report, provides a working understanding of potential repositories, traps, and sealing mechanisms that will be needed to design and implement a CO_2 injection project in the area of interest. As with most geocellular models, it incorporates geological information (stratigraphy, facies mapping, and structure) with estimates of critical flow parameters (e.g., porosity and permeability) at all locations. This model serves as the basis for the fluid flow simulations—a key exercise in predicting the potential for CO_2 injection and storage in the targeted aquifers.

Area of Interest

The Wabamun Area Sequestration Project (WASP) includes a region southwest of Edmonton, Alberta (Figure 1) with a total areal extent of approximately 5034 km^2. The area of interest (AOI) encompasses 60 townships (57.9 km × 96.6 km) of predominantly agricultural and recreational land. Four major coal-burning power plants are located in the northern portion of the study area (Figure 1) with more than 4000 MW total generating capacity between them. The AOI for WASP is expanded from a region previously identified as a potential site for geological storage of CO_2 (Hitchon, 1996; Michael et al., 2006; Michael et al., 2009).

Geological Setting

The sedimentary sequence for the WASP study area can be divided into Cretaceous and pre-Cretaceous (i.e., Mississippian, Devonian, and Cambrian) units, corresponding with an initial long period of passive margin deposition (blue-green layers on Figure 2), followed by the formation of a deep foreland basin (yellow layers on Figure 2). The combined Cretaceous and pre-Cretaceous intervals can be greater than 1500 m thick in the area of interest. The Paleozoic sequence is marine carbonate and shale dominated with passive margin sandstones found in the Cambrian basal unit. Cretaceous formations are mostly siliciclastics—sandstones, siltstones, and shales. All of the beds dip gently from NE-SW approximately 0.5 degrees on average through the study area.

In selecting aquifers most suitable for CO_2 injection, some key criteria are: (1) aquifer depth; the aquifer needs to be sufficiently deep to allow pressures and temperatures necessary for CO_2 to exist as a super critical fluid (i.e., 31.1°C and 7.8 MPa), but not so deep as to have little permeability (reservoir quality); (2) proximal barriers; there should exist multiple impermeable and low-permeability horizons (i.e., aquitards and aquicludes) between the target aquifer and the surface to minimize leakage risk; and (3) interference with existing activities; there should be no impact on existing hydrocarbon production. Using these simple criteria, the best aquifer targets in the WASP area are the Paleozoic passive-margin carbonates and basal Cambrian sandstones. A saline aquifer, the Devonian Nisku (Figure 2), is of particular interest as its depth, thickness, and stratigraphic configuration appear to be well suited for CO_2 injection and storage.

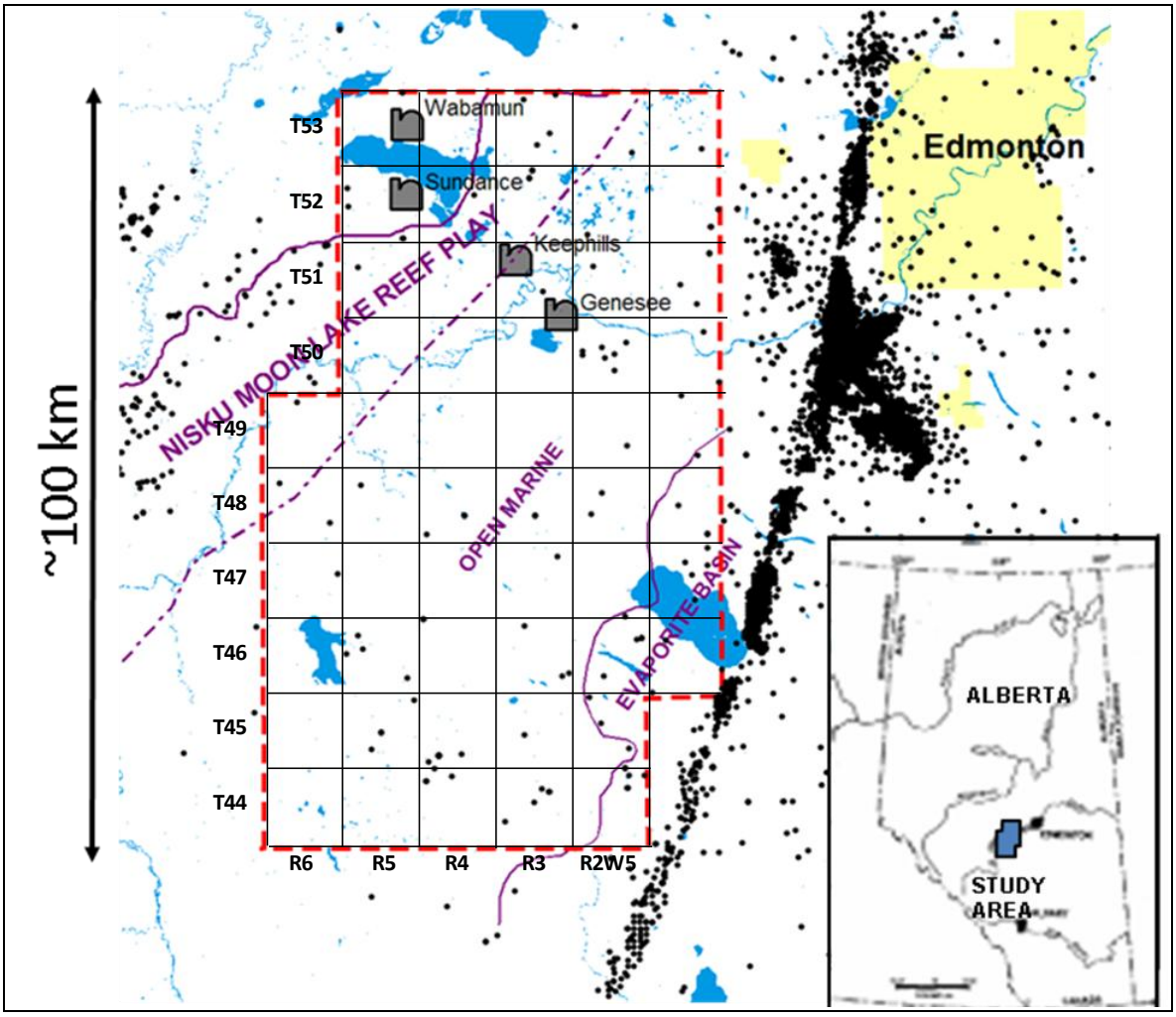

Figure 1: The WASP study area (red outline) and locations of four large power plants. Black circles show wells that penetrate the Nisku Formation. Purple lines mark important depositional boundaries of the Upper Devonian. The study area has an areal extent of approximately 5000 km^2.

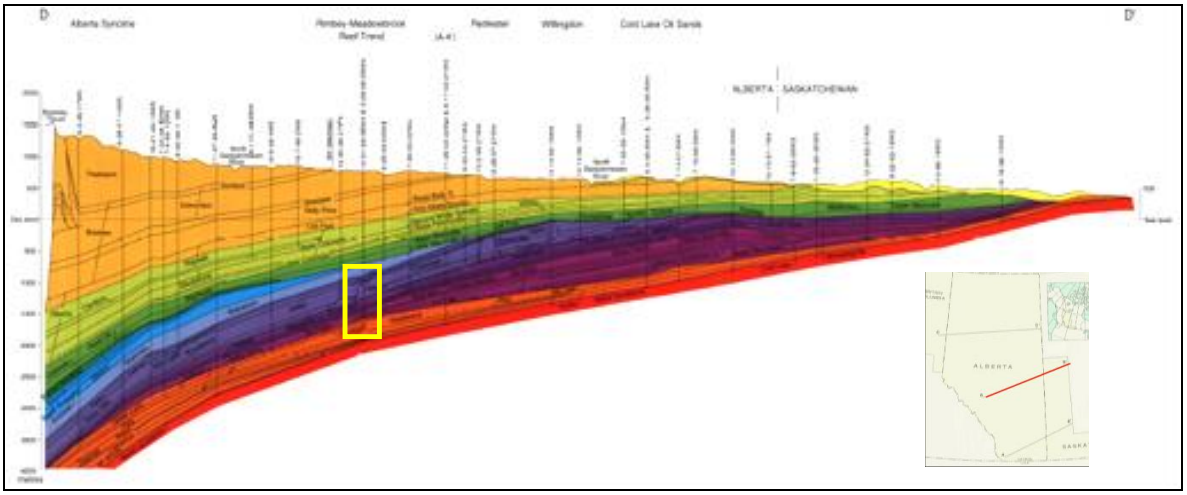

(Wright et al., 1994)

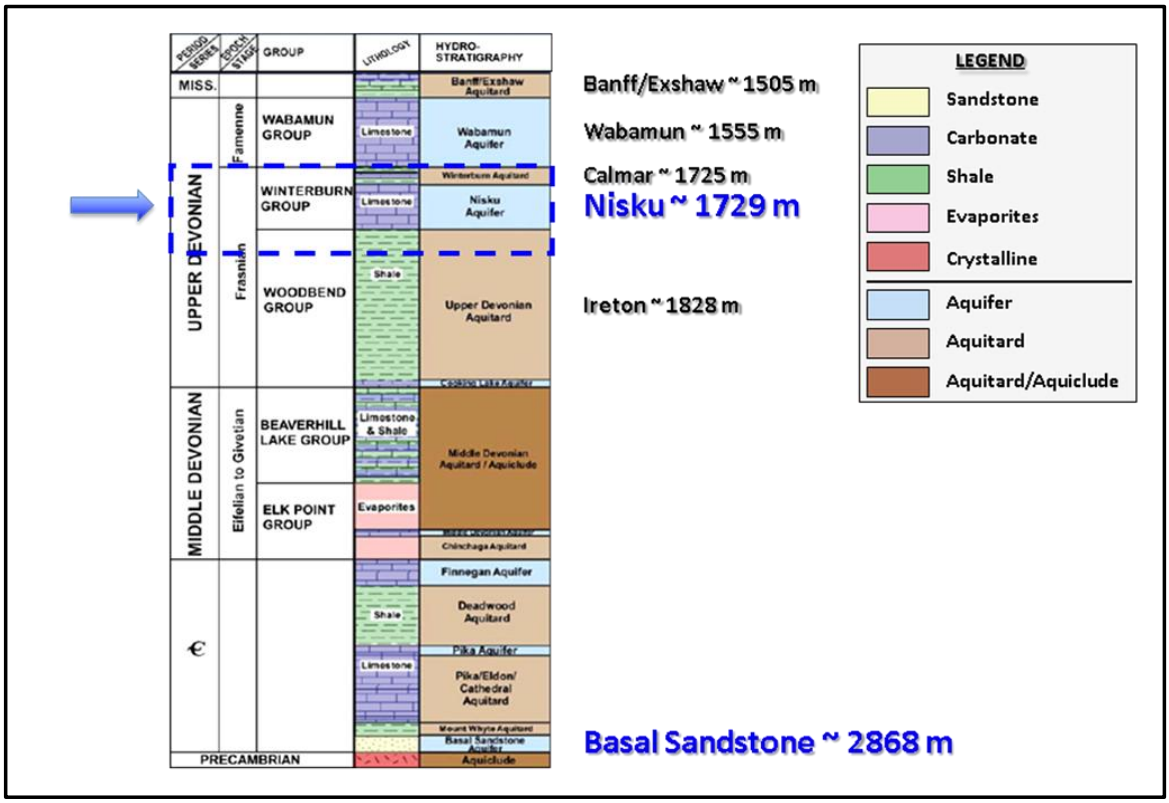

Figure 2: Geologic cross-section of the Western Canada Sedimentary Basin (Wright et al., 1994) showing Paleozoic interval of interest (yellow box). Stratigraphic column (modified from Bachu and Bennion, 2008) shows distribution of aquifers and aquitards. The target formation is the Upper Devonian Nisku carbonate.

Nisku Deposition and Lithofacies

Nisku deposition is part of the Winterburn Group after the last phase of the Woodbend Group sequence when the Western Canada Sedimentary Basin was nearly filled with shales and carbonates. The Nisku interval represents a strong marine transgression with carbonate ramp deposition dominant (Switzer et al., 1994). Indications suggest a late stage regressive episode as well, but deposition was diminished during this time in the area of interest (Switzer et al., 1994).

The WASP region includes open marine and more shallow, hypersaline carbonate ramp deposits within the Nisku stratigraphic interval (Figure 3). Thickness of the Nisku carbonate accumulation is shown in Figure 4, ranging from 40 m near the eastern boundary of the study area to over 100 m closer to the shelf margin. Basinward are hydrocarbon bearing pinnacle reefs (Zeta Pinnacle Trend) and shelf margin reefs (Moon Lake Build-Ups). These mark the western boundary of the potential injection aquifer. The eastern boundary is delineated by the transition from open marine carbonate facies to lower permeability hypersaline rocks of a paleo-evaporite basin (Figure 3).

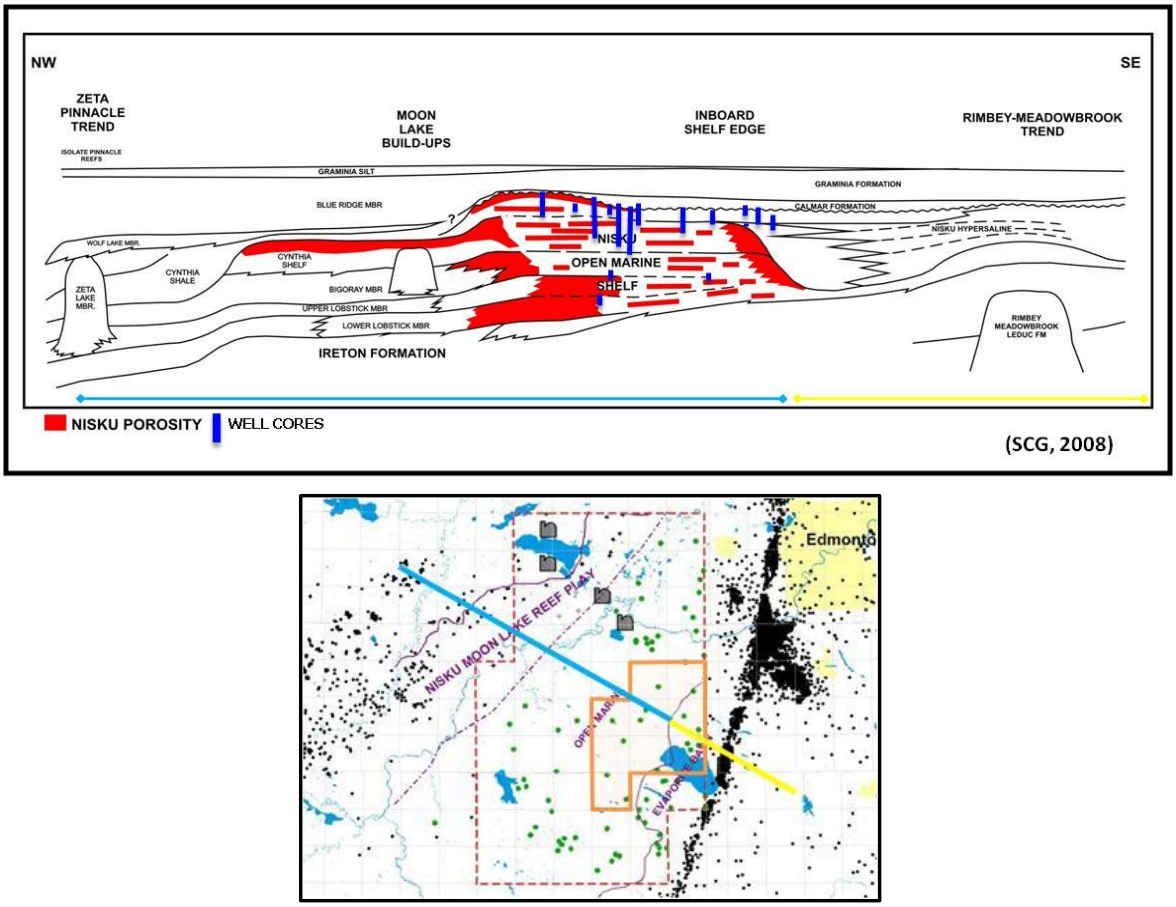

Figure 3: The top image shows a conceptual cross-section through the Nisku formation in the WASP study area. Red areas indicate larger expected porosity and vertical blue columns represent existing well cores. Most cores sample the upper portion of Nisku, where porosity is thought to be poorer. The map shows the outline of the entire study area (dashed red) and a high-grade focus area for seismic interpretation (solid orange). NE-SW cross-section line correlates with the above figure.

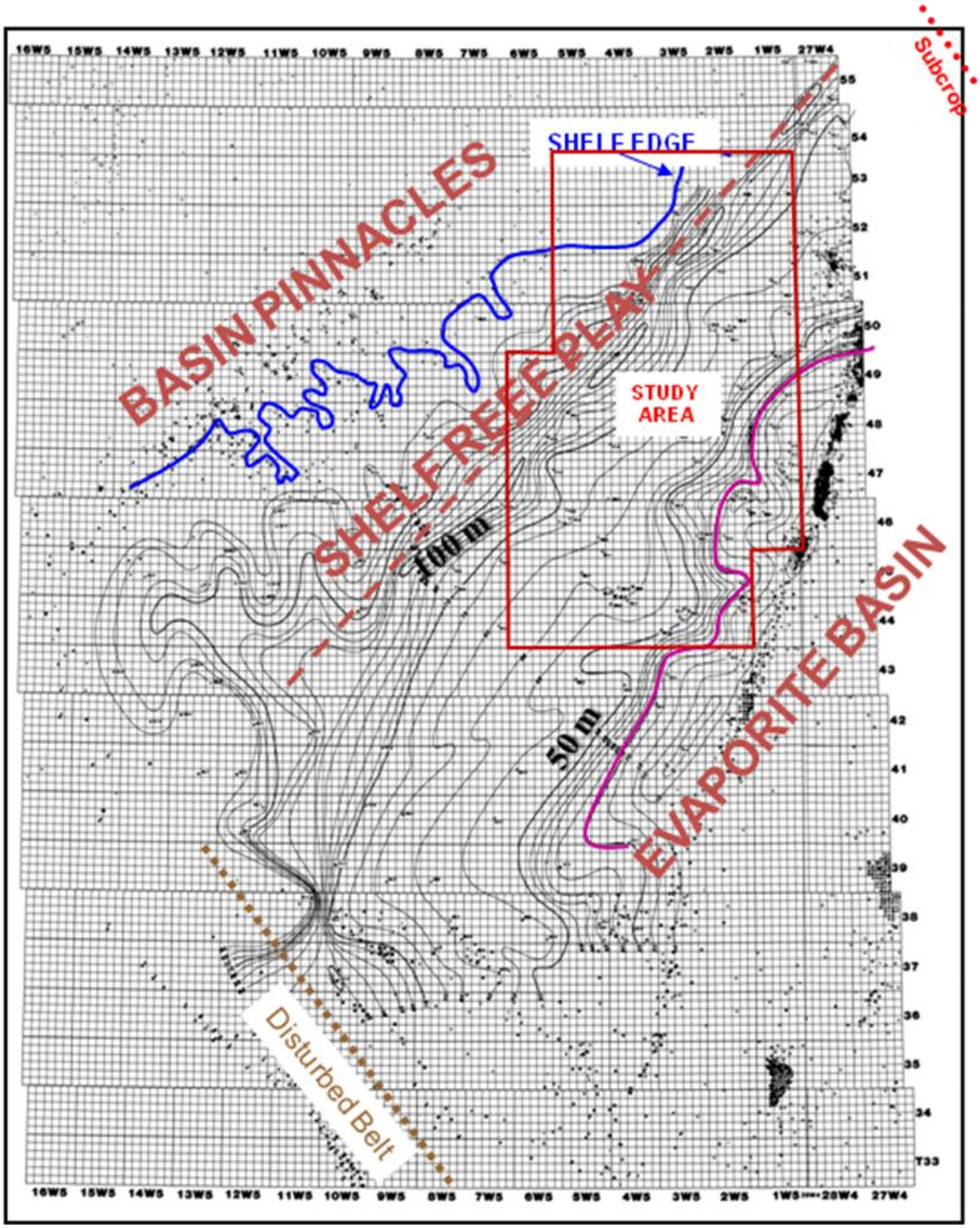

Figure 4: Isopach map (thickness) of Nisku carbonate (from SCG Ltd). Thickest portion is near the edge of shelf reef play with most areas between 50 and 100 m thick.

For the WASP study, two facies assemblages were recognized from the limited core available: an undifferentiated open marine carbonate and a hypersaline carbonate mudstone. The hypersaline facies (Figure 5) is comprised of dolomitic mudstone to grainstone with occasional moldic porosity and very limited Amphipora present. Abundant anhydrite and fine-grained silt and shale stringers reduce the permeability significantly. Measurements of core permeability are less than 5 mD and porosity is typically less than 2%. The open marine facies (Figure 6) includes dolomitic mudstone to boundstone lithologies. Vuggy and moldic porosity can be observed in some intervals. Anhydrite plugging is limited. Stromatoporoids and Amphipora are common, with less frequent corals and brachiopods also observed. From core measurements, porosities are typically between 3 and 5%, and permeabilities are between 5 and 15 mD. In more exceptional cases, porosity exceeds 12%, with permeability in the range of several Darcys.

The Nisku shelf is underlain by Ireton Fm. shales and overlain by fine-grained clastics of the Calmar Formation—a persistent, low-permeability shale unit typically between 5 and 12 m thick. Above the Calmar Fm. is the Graminia Fm. (inlcluding the Blue Ridge Member), which collectively with the Calmar comprise the Winterburn aquitard (Figure 2).

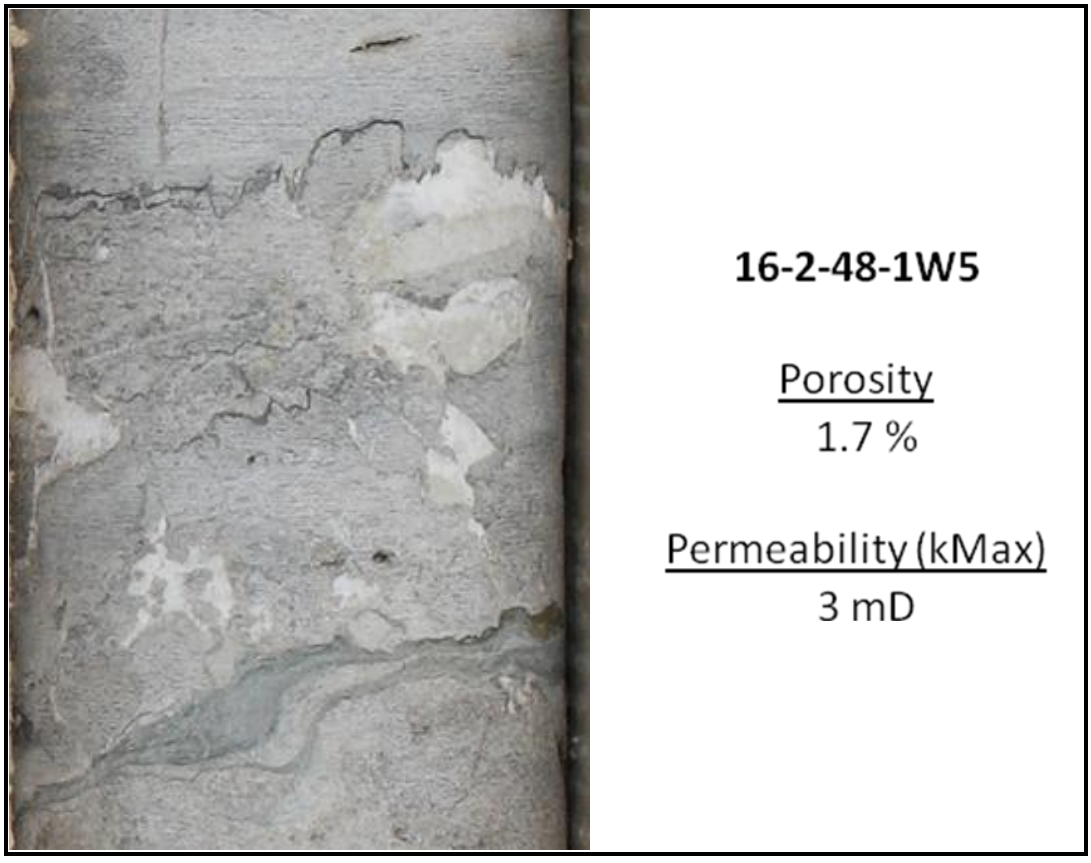

Figure 5: Sample of typical hypersaline facies. Dolomitic mudstone to grainstone with anhydrite plugging are evident.

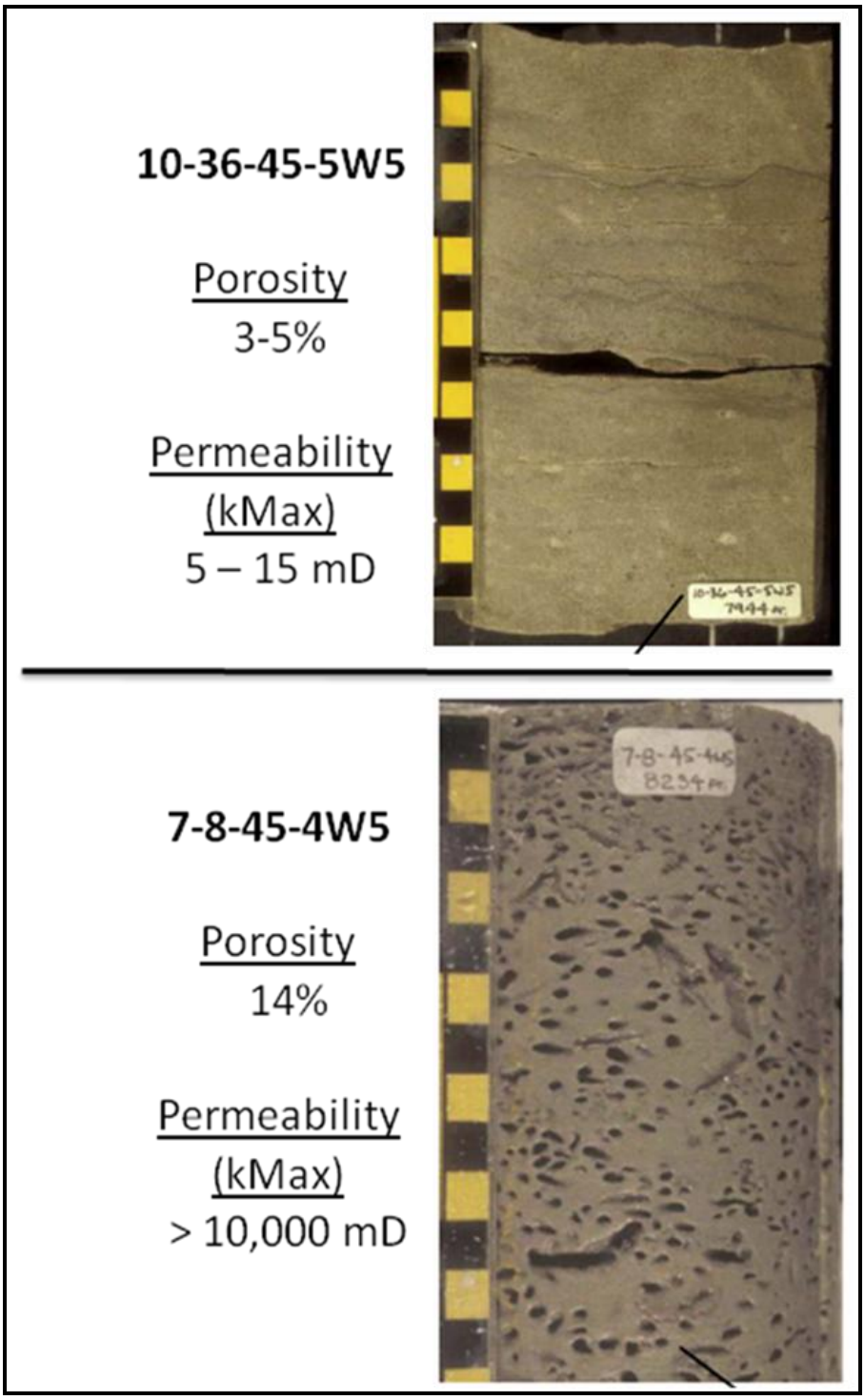

Figure 6: Samples of open marine facies of Devonian Nisku Fm. Typical carbonate (top) versus carbonate with exceptional porosity and permeability (bottom). High porosity example (bottom) shows evidence of abundant Amphipora. Core photos courtesy of SCG Ltd.

1. DATA

The static earth model comprises characterizations of facies, porosity (ϕ), and permeability (k) in the WASP study area. The static model then feeds into dynamic models for fluid flow and geomechanical simulation. Information used for creation of the static earth model includes:

- Data from 96 wells that penetrate the Nisku within the WASP AOI.
- Wireline geophysical logs of varying vintage, from the 1950s to recent suites.
- Routine core analyses and lithological descriptions for 13 wells in the study area. Special core analyses for select samples.
- Processed and raw geophysical data.
- Drill stem tests (DSTs) of generally poor quality.
- Petrographic studies, both publicly available and newly completed for this study.

All core, geophysical, seismic, geomechanical, geochemical, and other relevant data sets used for this study are collected in a digital database maintained with the Energy and Environmental Systems Group (EESG) at the University of Calgary.

The distribution of these sparse data presents a challenge for accurate modelling in the inter-well zones (Figure 7). Cored wells only cover approximately 10% of the WASP area, and inter-well distances are on the order of ~0.5 km to >20 km.

1.1 Wells

For each well drilled, information is provided about the location and depth, the historical status of operation, and in some cases, well casing and completion. Production data are scarce for the Nisku interval as very few wells have produced. One notable exception is a currently active water-production well (F1/11-29-045-02W5/00), which has data recorded since January 2003. A list of wells and selected information are provided in Appendix 1. The entire database is available digitally in the WASP project archives.

1.2 Core

Thirteen wells that include core for some portion of the Nisku interval in the AOI (see Figure 7 and Appendix 2) were logged. Cores are typically 1", 3", or 4" diameter, and represent a small portion of the Nisku interval, usually <20 m. Prior to this study five wells included core with routine core analysis. For this project, cores from eight additional wells were sent for routine analyses. Core plugs provided measurements of porosity, permeability, and in most cases grain density. Two of these wells were outside the study area (Figure 7). Special core analyses (directional permeability and compressibility measurements) were obtained for a subset of collected cores.

All available cored sections were logged by SCG Ltd. and are stored at the ERCB's Core Research Centre in Calgary, Alberta. Core descriptions and photographs are available in the WASP project archives.

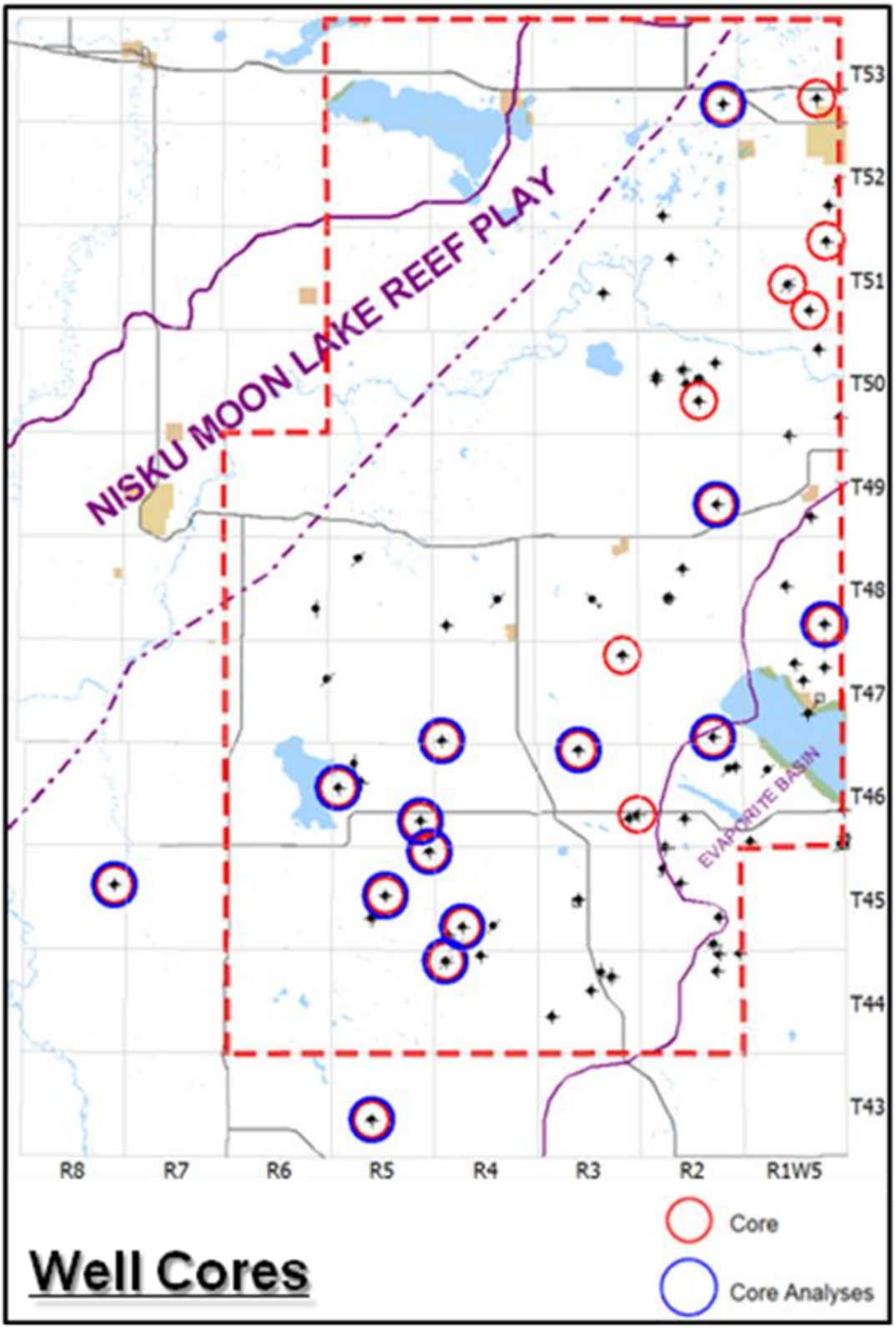

Figure 7: Distribution of available well cores from the Nisku. Core analyses from existing (5 wells) and newly acquired (8 wells) data sets.

1.3 Wireline Geophysical Logs

Logs exist for 93 of the 96 wells in the study area. Log type and quality largely depend on the vintage:

Number of Wells	Vintage	Types of Available Logs
35	Pre-1960	SP, resistivity
34	1960–1980	resistivity, porosity
24	Post-1980	full suite

Of these 93 wells, digitized logs for 79 wells were used in the analysis and interpretation (see Appendices 1 and 3). Wells drilled into the Moon Lake play (17 in total) were excluded so as to avoid mischaracterizing reservoir properties in areas away from this play. An additional two wells that penetrate the Nisku outside the study were also used for modelling as they allowed core calibration in lower Nisku intervals. Of the digitized logs, depth sampling intervals varied between 0.1 m, 0.15 m, 0.2 m, 0.5 m, and 0.6 m. All digitized logs were re-sampled at 0.5 m or 0.6 m.

A critical step before petrophysical analysis is quality control of the digitized wells—this involves checks for unit consistency and accuracy, depth shifting (where possible), and general comparisons with the raster copies for errors in scaling and/or digitization. All of the available logs were imported into the Schlumberger modelling software for analysis.

Stratigraphic picks were made by SCG Ltd. geologists, primarily based on geophysical logs with Nisku facies distinctions influenced by core observations and facies isopach mapping. All stratigraphic picks were individually verified to assure consistency in mapped surfaces.

1.4 Seismic Data

The availability of seismic data is shown in Figure 8. There are a total of 199 2D lines, and seven 3D volumes acquired between 1980 and 2003. Data processing and interpretation was focused on a subset region (purple outline in Figure 8 map). This region was selected based on available seismic data, proximity to potential point source emitters, and a general understanding or the area geology. While this data set provides useful coverage in the focus area, more 3D volumes are needed for a seismic characterization of the entire WASP AOI.

Seismic data have a number of valuable characterization roles. In addition to basic interpretations of the Nisku structure via seismic travel time and amplitude, it is also possible to use other attributes, such as acoustic impedance, to examine the physical nature of the Nisku interval for insight regarding physical properties of the rock.

Seismic 3D volumes were incorporated for use in the geomodelling process. Detailed information on seismic processing and interpretation is described in the full report by Alshuhail et al.

1.5 Mineralogy

A mineralogical evaluation of select core samples was completed. Analysis methods include XRD, XRF, and electron microprobe, as well as standard petrographic assessment. Details and results of this work are presented in the geochemistry section of the full report.

1.6 Drill Stem Tests

Twenty-two DSTs of generally poor quality have been recorded for the Nisku aquifer (Figure 9). The details of these measurements are available in Appendix 4. The recorded DST measurements were difficult to use for a number of reasons including no (or low) resolution of data, erroneous reservoir pressures and temperatures, 'stair-stepping' of data points, and erratic pressure plot derivatives. Quality of the DSTs was subjective based on an assessment of data points for a given DST, as well as a rating system devised by Hydro-Fax Resources Ltd.

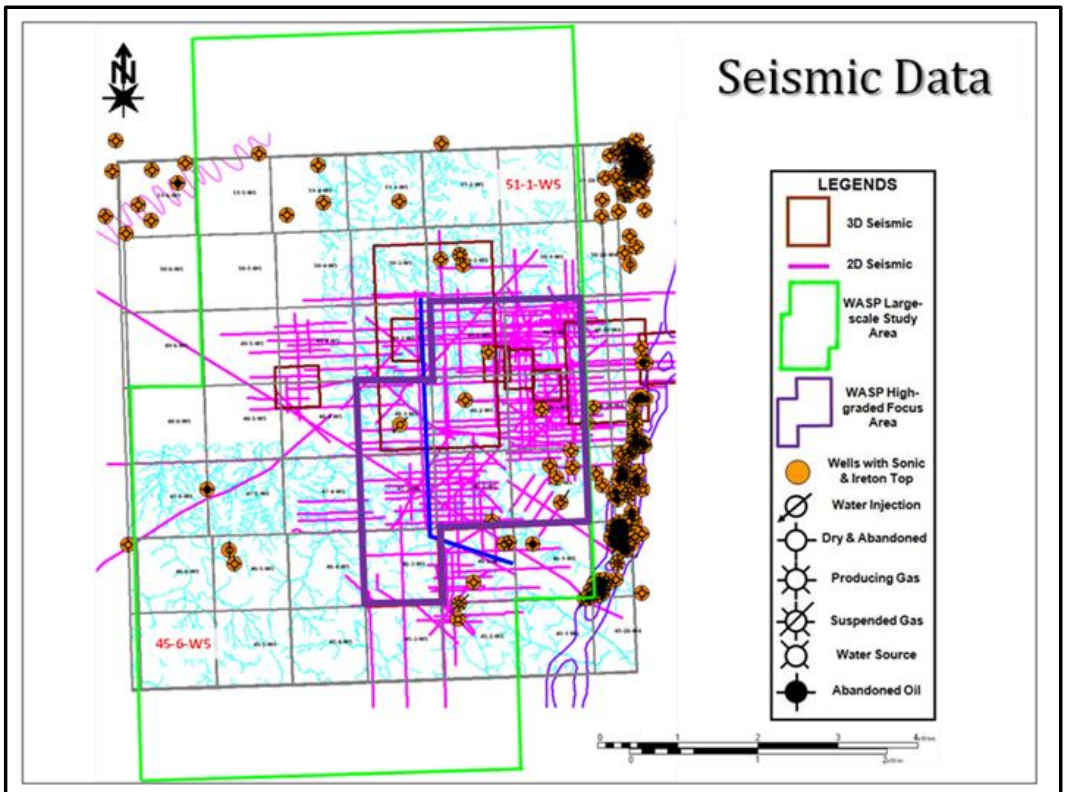

Seismic data	2D	• 199 seismic lines. • Length: 2432 km.
	3D	• 7 seismic volumes. • Area: 419 km².
Borehole data (sonic + Ireton top)	Within HGFA	• 7 wells within the seismic coverage inside the high-grade area. • 3 wells within the 3D volumes.
	Nearby HGFA	• > 7 wells near seismic coverage near the high-grade area. • 4 wells within 3D coverage. • Limited aperture.

Figure 8: Available 2D and 3D seismic data for WASP study. Map (top) shows distribution relative to study area (green) and high-grade focus area (HGFA) (purple). For further information refer to geophysics chapter of report.

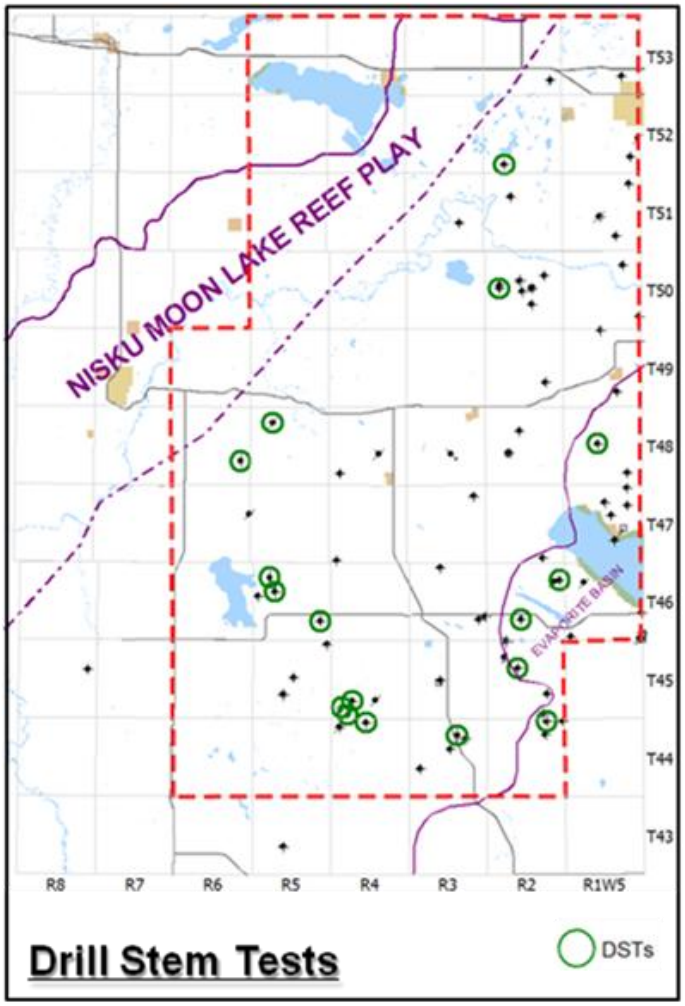

Figure 9: Distribution of DSTs within WASP study area (green circles).

Analyses of DST data are useful for assessing potential reservoir pressures, behavior over time, and most importantly providing estimates of flow capacity (i.e., permeability × thickness). Horner plot analysis was used to estimate these parameters. A summary of the analyses are described in Table 1 and Appendix 4. Additionally, DST estimates of flow capacity can be used as a rough validation tool for gauging the accuracy of static earth models used for flow simulation. DSTs targeted only limited intervals of the Nisku Fm. (Appendix 4).

Table 1: Summary of DST analyses from Nisku interval in WASP region.

Description	Results
Number of DSTs	22 (18 for k estimation)
Quality	poor to mediocre
Permeability (k) est. (mD)	<0.01 – 74
Permeability thickness (kh) est.(mD-m)	<.1 – >700
Initial reservoir pressure est. (kPa)	~15,000 – >21,000
Fluid recovery column (m)	114 – 1963

2. PETROPHYSICS

With limited data from direct geological sampling (i.e., core and cuttings), wireline geophysical well logs provide a critical source of information for characterizing the reservoir of interest. The logging process, while providing a complete vertical view of the target interval, requires a significant degree of interpretation in order to provide the necessary data for geological modelling and flow simulation.

For the Nisku Formation in the Wabamun study area, a wide range of logs have been acquired during the past 60 years (see Appendix 3). Many of these logs were recorded digitally, but at a variety of sampling intervals (e.g., 0.5 m, 0.2 m, and 0.15 m). Calibration of these data is critical, as is quality control to ensure reliability and accuracy.

Described in this section are the general steps followed for quality control and calibration of well logs. Then an analysis of porosity measurements will be presented, followed by the techniques developed for estimating permeability.

2.1 Well Logs

Digitized wireline logs were imported into Schlumberger's Petrel geomodelling software. Effort was taken to ensure the digitized well logs were imported in consistent units (metric) and that digital values matched the raster-based logs for the intervals of interest. In some cases the scaling of digital well logs needed to be corrected. An example comparison between digitized and original raster sonic-log for the Nisku interval is shown below:

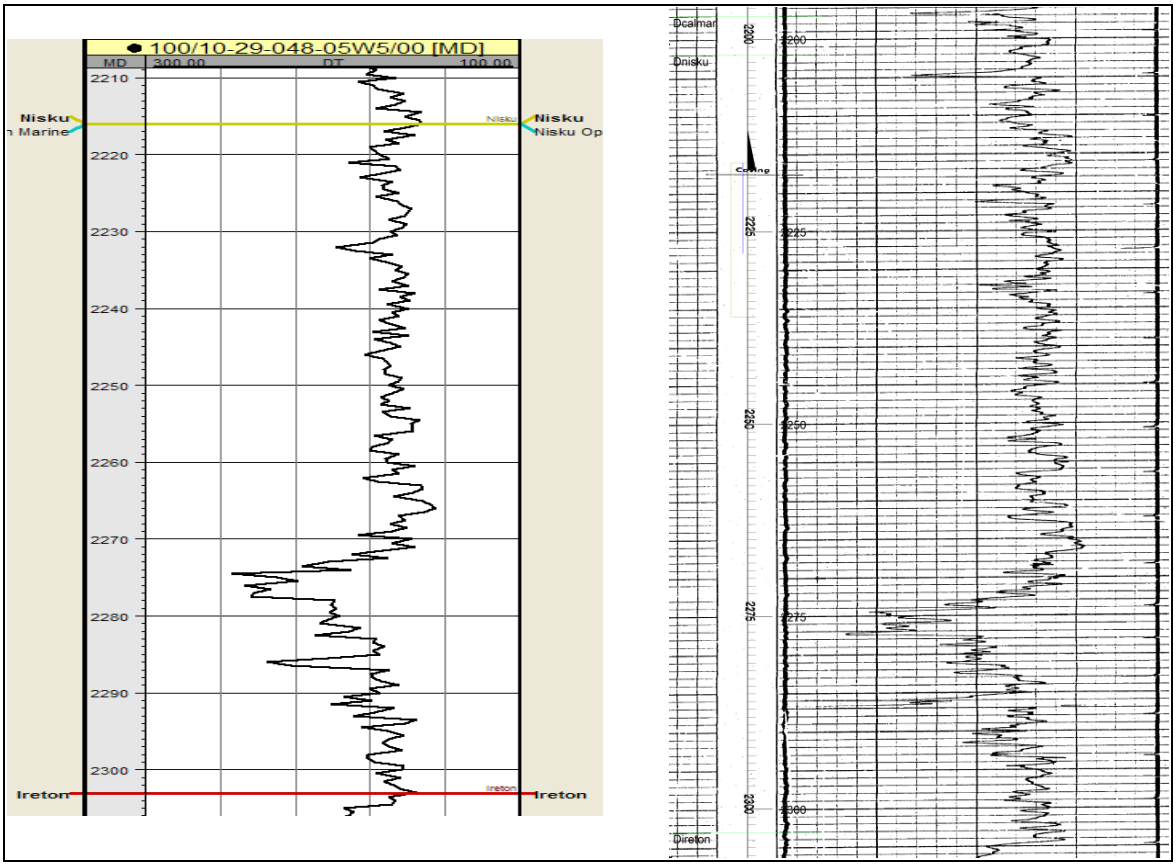

Depth shifting was performed where coincident core was available (Appendix 1). The principal method was to compare the depths of core porosity with log porosity, and shift the former to the match the latter. Accuracy of 0.3 metres or less was the objective.

2.2 Porosity Estimation

For traditional oil and gas exploration, porosity is usually estimated quantitatively from sonic, density, and neutron wireline data. Resistivity (or conductivity) measurements are more often used for semi-quantitative estimation only. In the case of deep saline aquifers, resistivity may provide useful quantitative estimates due to the assumed 100% water saturated formation environment.

Sensitivities to porosity in carbonate lithologies is not straight forward, although it is generally assumed that acoustic methods are more sensitive to separate-vug porosity, whereas neutron and density logs estimate total porosity.

2.2.1 Core

Petrophysical data obtained from core measurements are normally considered to be accurate and are used to calibrate log data. With limited coverage of the Nisku interval, core provides only a rough estimate of key physical parameters for the entire reservoir, and necessarily needs to be supported by the available wireline data

A summary of the core porosity data, obtained for 13 wells (Appendix 2), is shown in Figure 10. The data are mostly from the less porous, uppermost parts of the open marine facies.

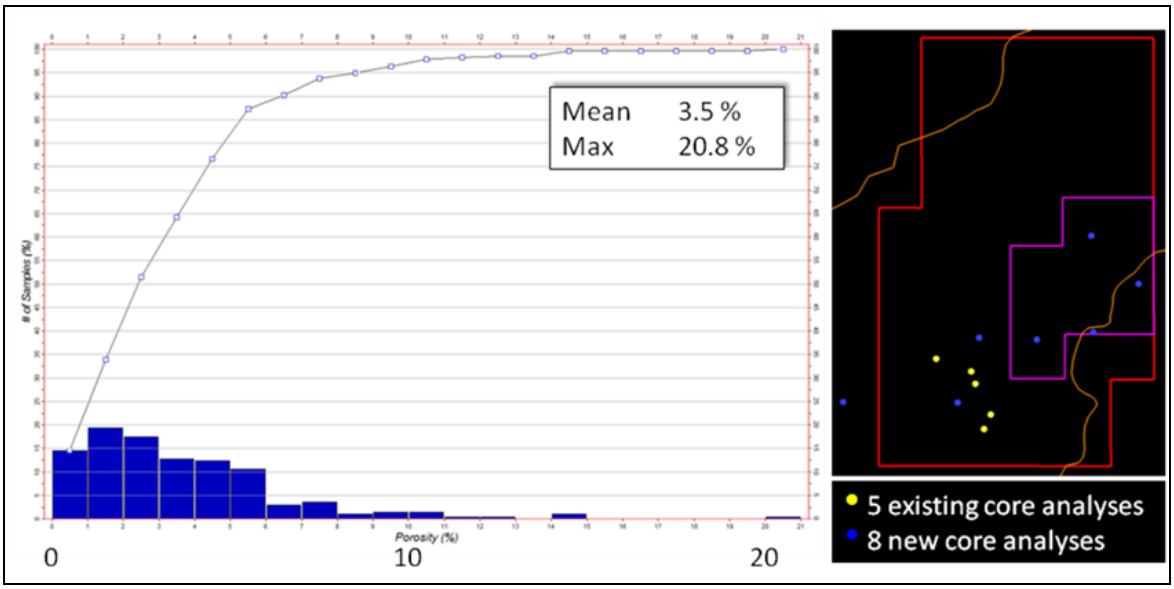

Figure 10: Core porosity data and sample locations.

2.2.2 Acoustic Wireline Logs

The capacity to transmit sound waves varies with lithology and rock texture, in particular porosity. For the WASP study, there exist 32 wells with sonic logs available (Figure 11). Porosity was quantitatively calculated from these data assuming the relationship of Wyllie et al. (1956):

$$\phi_s = \frac{\Delta t - \Delta t_{ma}}{\Delta t_L - \Delta t_{ma}}$$

Where ϕ_s = porosity; Δt = tool measured interval transit time; Δtma = transit time of matrix material; and ΔtL = transit time of interstitial fluid. The assumed values for the Nisku carbonate are Δtma = 143 µsec/m (suitable for a dolomite) and for the Nisku aquifer fluid, ΔtL = 623 µsec/m.

In the cored intervals, the vast majority of samples included mostly interparticle porosity with occasional moldic porous zones. The separate-vug porosity was generally less than a few percent of the total porosity, so the Wyllie time-average could provide useful estimates (Lucia, 2007). On comparison of the core porosity and ϕ_s (Figure 11), the sonic porosity tends to overestimate core porosity. This may be caused by anhydrite in the cored intervals, which has a larger transit time (164 µsec/m) than that assumed for ϕ_s.

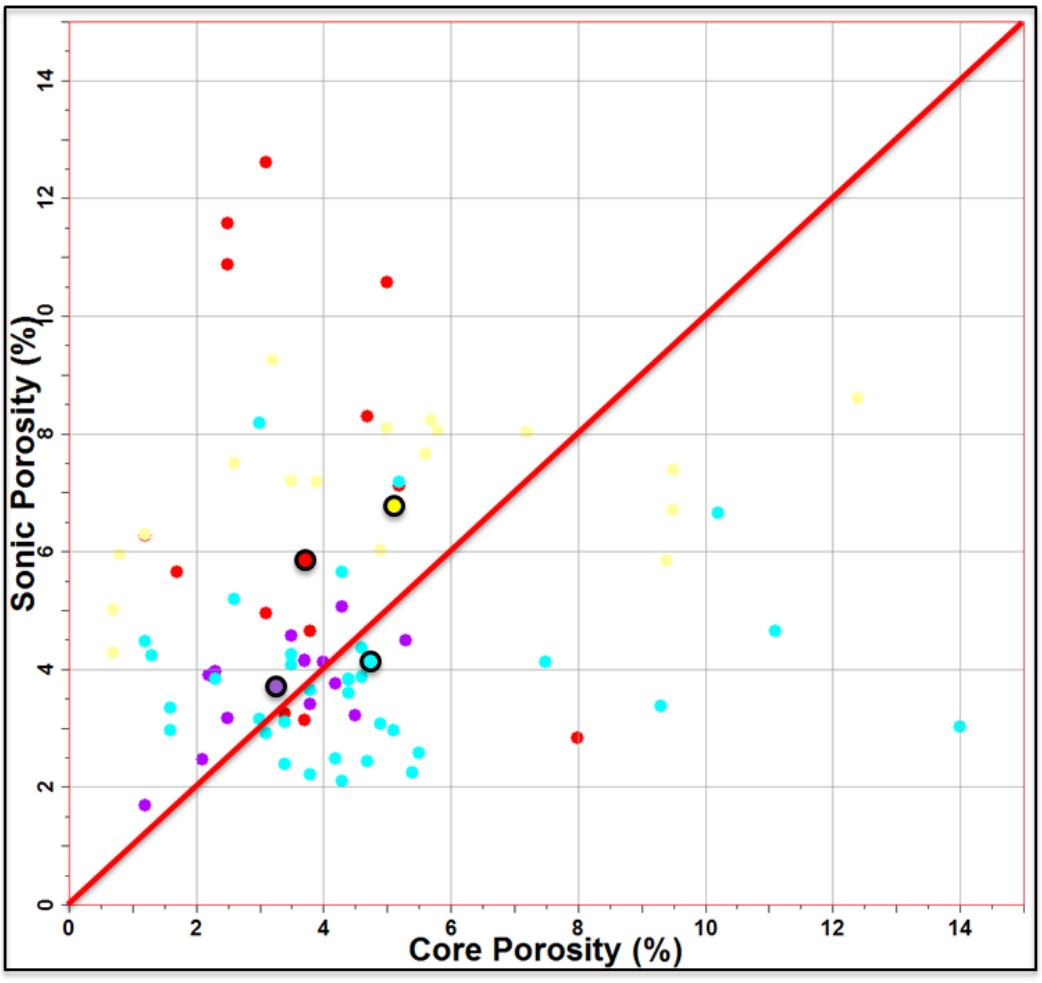

Figure 11: Cross-plot of core porosity estimates versus acoustic log estimates. Larger circles represent mean values for each well (shown in different colours).

2.2.3 Density and Neutron Wireline Logs

Porosity is commonly calculated from a combination of estimates made using neutron and density logs. The general form in water-bearing formations is:

$$\phi_{DN} = \left(\frac{\phi_D + \phi_N}{2}\right)$$

where ϕ_D = density porosity (lithology corrected) and ϕ_N = neutron porosity (lithology corrected).

For WASP, there were 13 wells containing coincident density and neutron logs (Figures 12 and 13). In addition to estimates of porosity the density-neutron combination is an important lithology indicator (Figure 13), suggesting most of the samples for the Nisku are dolostone. There are also occasional occurrences of limestone and silty-mudstones.

The ϕ_s values are less variable than the density-neutron porosities (Figure 12). Possible reasons include:

1) the amount of moldic and vuggy porosity is highly variable and larger overall than revealed in core, so that, as in Figure 14, the sonic underestimates the total porosity in vuggier portions of the reservoir;
2) the density-neutron porosity estimates are more robust to anhydrite than the sonic; and/or
3) more wells in the hypersaline facies are logged with sonic than density-neutron and the hypersaline has smaller porosity than the open marine facies.

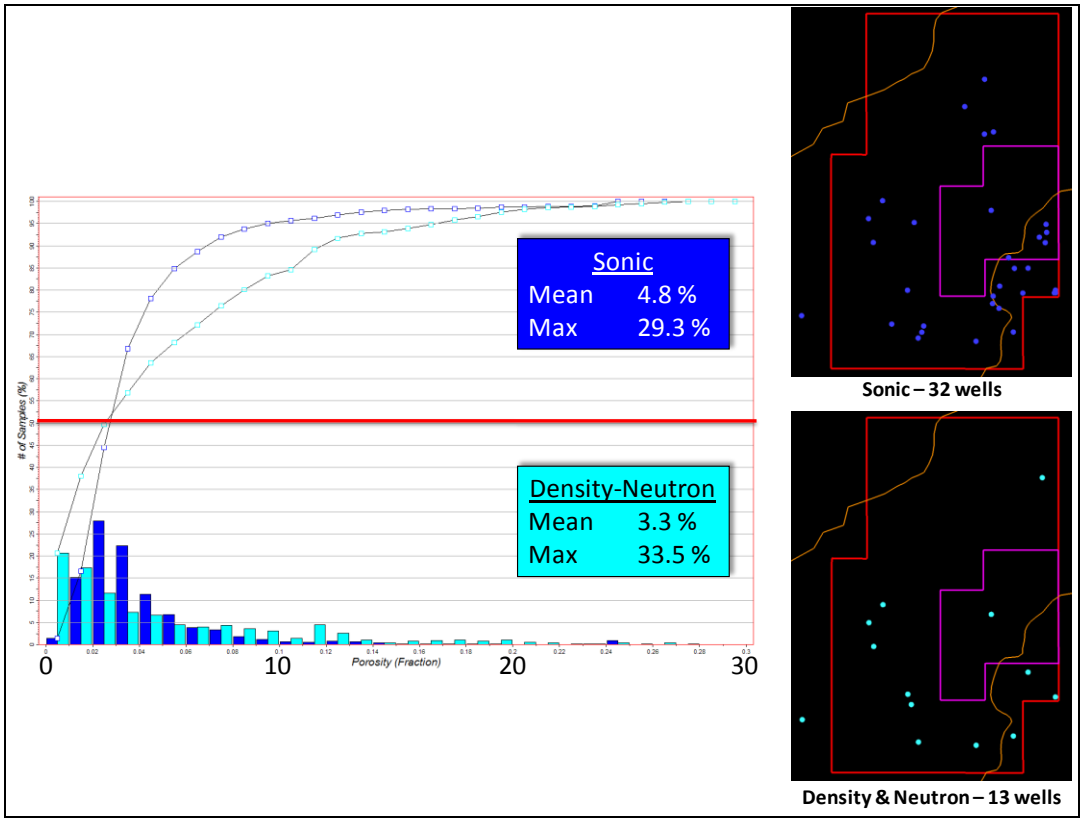

Figure 12: Porosity determinations from acoustic and density-neutron wireline logs. Locations for samples shown on right.

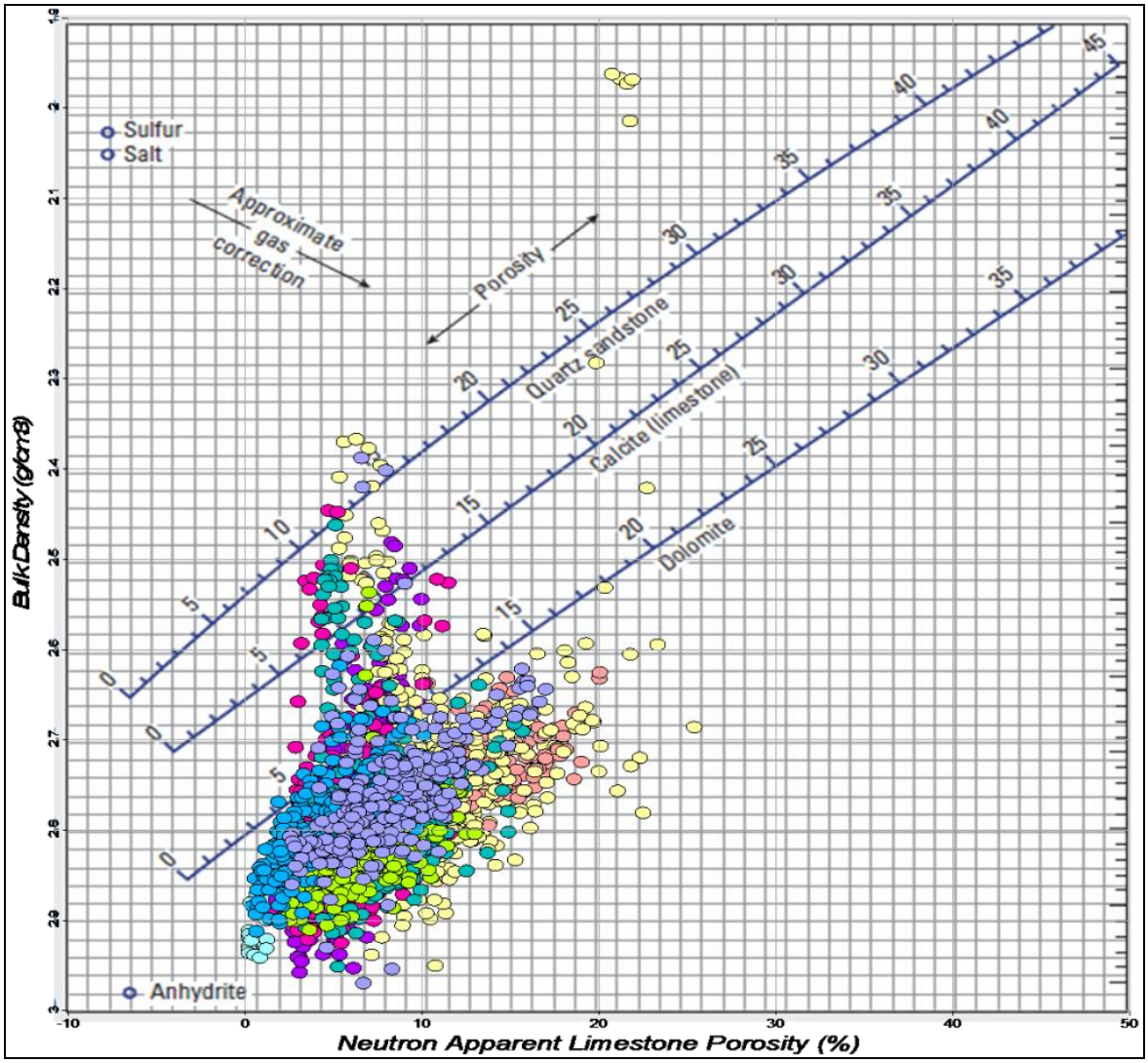

Figure 13: Porosity and lithology determination from bulk density and compensated neutron logs. Nine of the 13 neutron logs used for this plot were run prior to 1986, so the dolomite response line for these logs is more curved concave up than the one shown here.

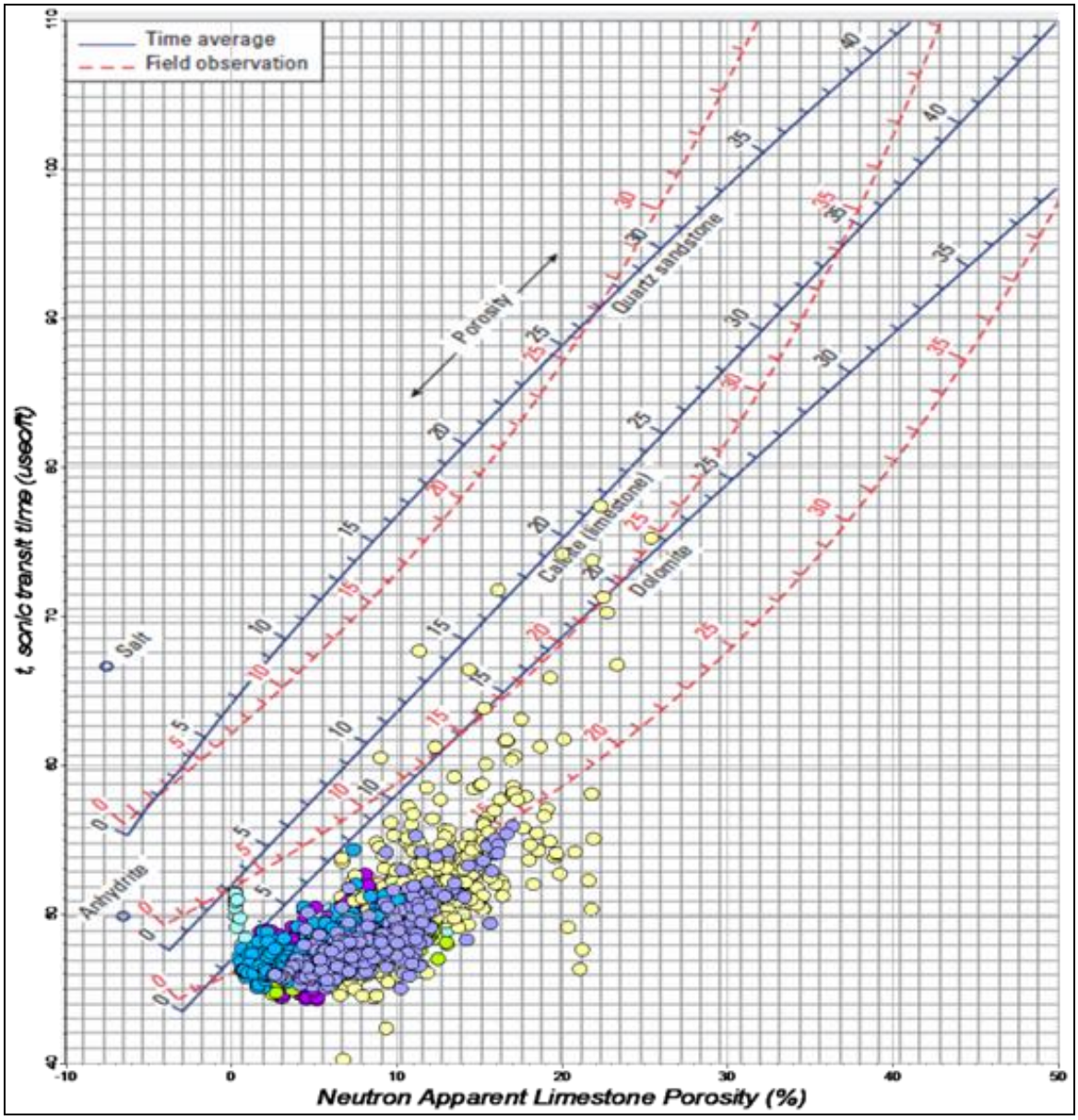

Figure 14: Porosity determination from acoustic and compensated neutron logs.

2.2.4 Resistivity Wireline Logs

There are just over 50 wells which have deep resistivity or conductivity logs distributed over a more extensive portion of the WASP study region (Figure 15). While restitivity logs were run to find hydrocarbons, they also have a potential quantitative utility in describing porosity and permeability in the case of saline aquifers.

Archie (1942) proposed that in 100% water-saturated rocks, porosity depends on rock resistivity (Ro), water resistivity (Rw), and the pore geometry/cementation factor (m):

$$\phi^{-m} = \frac{R_o}{R_w}$$

This relationship is valid for a deep-saline aquifer because S_w is at unity. The formation water resistivity (R_w) was established to be 0.029 ohm-m based on direct measurements from a water source well (11-29-045-02W5) in the Nisku and other R_w measurements collected during drilling (Appendix 5). R_o was estimated using the deepest resistivity measurement available in the log suite (e.g., deep induction). No environmental corrections were applied to the resistivity log values.

Using wireline measurements from deep induction and density-neutron logs, it was observed that $2 < m < 3$ (Figure 16). A similar range for m is obtained using core porosities (Figure 16). This range is consistent with values of m obtained in other carbonate formations (e.g., Lucia, 2007, p. 72). Once a range of values for m is established, porosities may be estimated from the deep resistivity log measaurements. For example, at 10 ohm-m, estimates of porosity range from 5.3% to 10.5% (Figure 16).

Assuming m = 2.5, resistivity thresholds were established to map out potentially good porosity intervals (Figure 17). For this particular cross-section of wells, lower resistivity zones that have ϕ > 8% appear most common in the lower third of the Nisku stratigraphic interval, with fewer zones in the upper third and very few zones in the middle third.

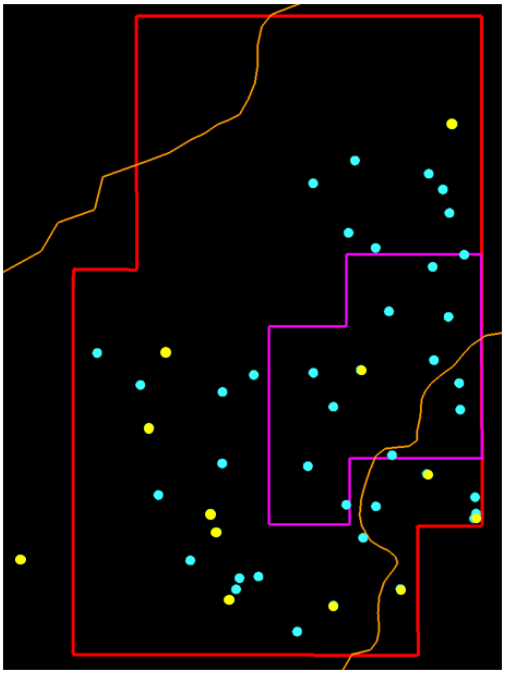

Figure 13: Distribution of deep resistivity and conductivity logs in WASP area. Yellow circles indicate wells with coincident density-neutron logs.

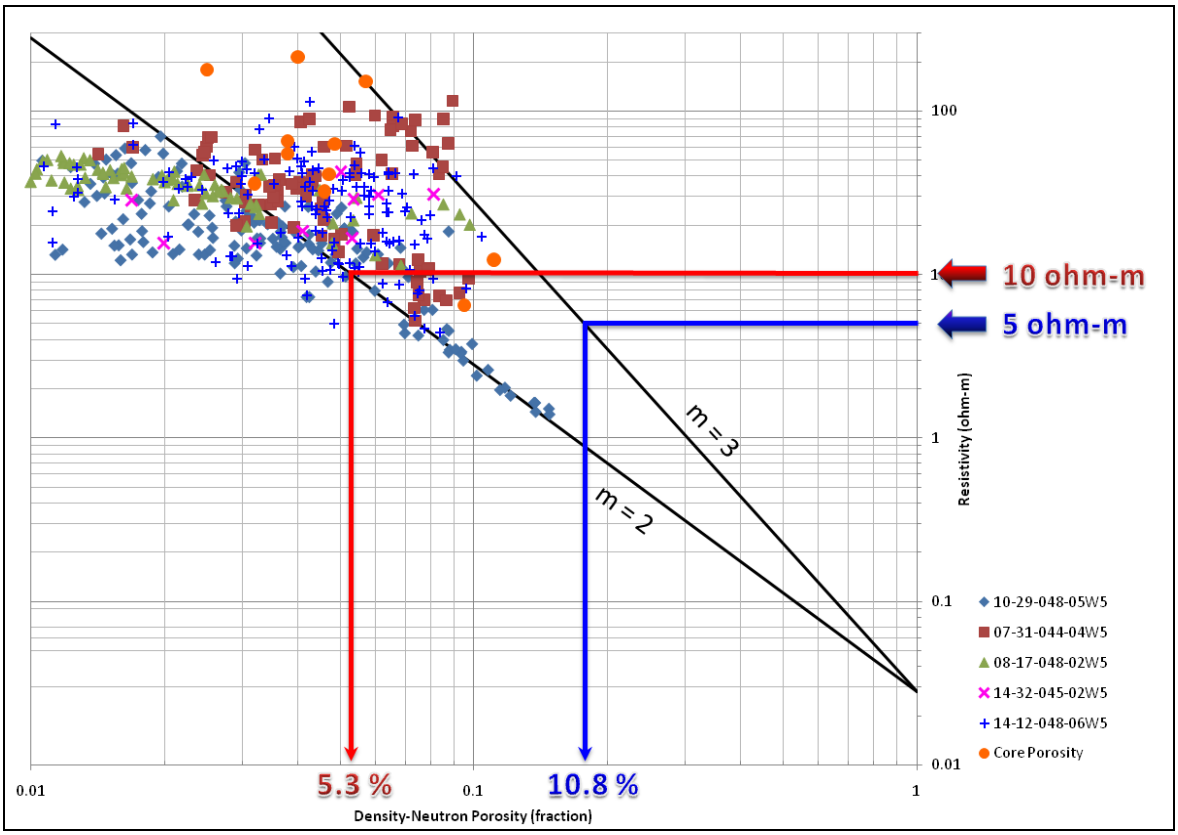

Figure 14: Relationship between deep resistivity data and porosity based on Archie's Law. Cementation factor (m) likely between 2 and 3.

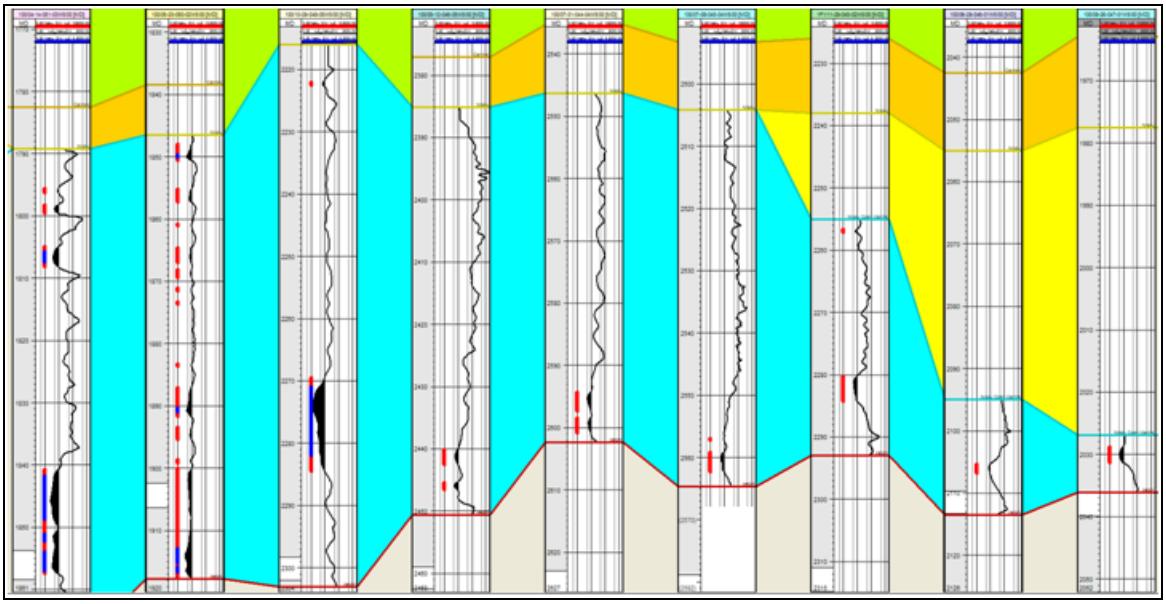

Figure 15: Intervals of enhanced porosity (<10 ohm-m [blue] and <5 ohm-m [red]) are shown on a cross-section of deep resistivity logs. There is a concentration of higher porosity zones in lower third of Nisku interval.

2.2.5 Porosity—Summary

- Resistivity-based porosity prediction is a useful way to use wireline resistivity logs, which are more numerous than sonic, density, an neutron logs.
- Cementation factor (m) appears variable between 2 and 3.
- The porosity-resistivity relationship suggests:
  - (1) <10 ohm-m correlates with > 5% porosity
  - (2) <5 ohm-m correlates with > 8% porosity
- Analysis of resistivity logs for select wells suggest:
  - (1) Areas located in central portion of Nisku platform have potentially good porosity.
  - (2) Porosity enhancement towards the base of Nisku formation.

2.3 Permeability Estimation

Permeability is a critical flow parameter for quantifying the potential for CO_2 injectivity. Despite its importance, there are relatively few permeability assessments for the Nisku. Permeability data exist for the limited core samples acquired, but not necessarily at reservoir conditions. Some variable-quality DSTs are also available, along with production data from well F1/11-29-045-02W5/00 and oil fields in the Leduc trend north east of the AOI. All these data have been analyzed to develop flow capacity estimates.

2.3.1 Core

A histogram of core permeability measurements suggests core-scale permeabilities are highly variable (Figure 18). The lower and upper values observed are likely to reflect measurement limitations as well as the intrinsic permeability of the rock. These were obtained from 13 wells with core collected from the Nisku (Appendix 2). The median permeability is nearly 10 mD, although these data represent a small fraction of the total Nisku interval. Core kh for 7 wells from the uppermost Nisku (Figure 19) suggests potential aquitard qualities—more than 75% of the measurements are below 10 mD-m.

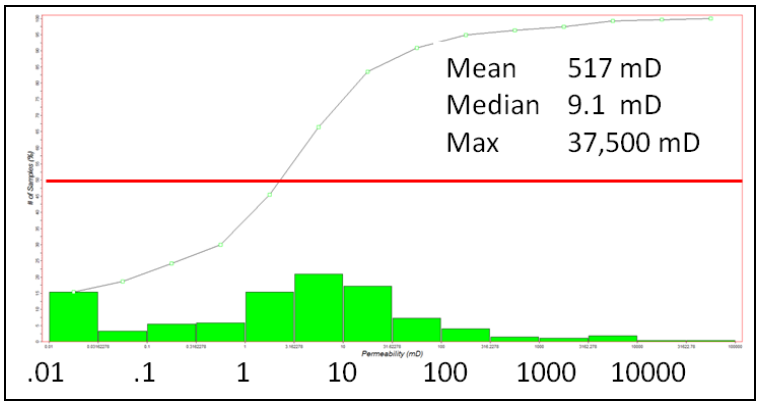

Figure 16: Core permeability measurements (kMax) from the 13 wells with Nisku sampling.

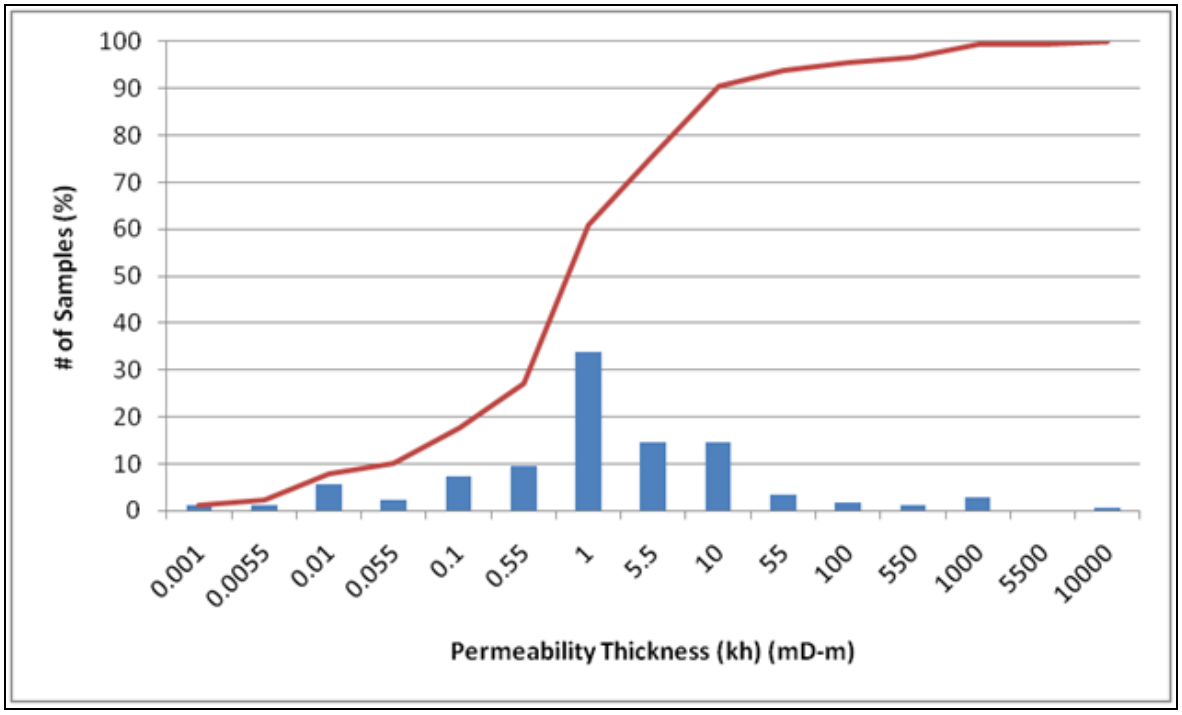

Figure 17: Core-measured permeability × thickness (from 7 wells).

2.3.2 Well Tests

DST measurements provide estimates of permeability at a scale larger than those provided in core plug measurements. The data, while of questionable quality, can provide a gross validation of flow capacity potential for a given well and the aquifer in general.

For individual well tests, the following permeability-thicknesses (kh) were estimated using a horner plot analysis method:

Well Location	kh (mD.m)
100/02-21-048-01W5/00	204
100/04-20-050-02W5/00	153
100/05-12-046-05W5/00	<1
100/06-05-045-04W5/00	16
100/07-08-045-04W5/00	293
100/10-09-046-02W5/00	99
100/10-14-053-03W5/00	3
100/10-20-046-05W5/00	69
100/10-27-044-03W5/00	35

Well Location	kh (mD.m)
100/10-33-044-04W5/00	68
100/13-36-053-03W5/00	99
100/14-21-045-02W5/00	719
100/14-21-045-02W5/00	6
100/14-29-046-05W5/00	<1
100/15-35-044-02W5/00	<1
102/16-06-045-04W5/00	16
102/16-06-045-04W5/00	13

2.3.3 Analysis of Production Data

The Nisku formation provides aquifer support for a number of oil fields to the northeast along the Rimbey-Leduc trend (RLT). Analysis of the production for several fields, detailed in the section on aquifer material balance, indicates the flow capacity of the Nisku in the north east may be approximately 200 to 500 mD-m. Using these values to evaluate flow capacity in the AOI, however, requires caution because of the change in depositional environment from the RLT to the open marine facies in the AOI. The two wells in the study area closest to the aquifer supported plays, 02-21 and 04-20 (see list above), have kh values at the minimum range established from material balance estimations.

The water production well, F1/11-29-045-02W5/00, has reported production capabilities of 1000 m^3 per day. Assuming a 10 cm radius wellbore and 10% pressure drop to produce a flow of 1000 m^3 per day, we estimate the formation flow capacity to be approximately 3000 md-m.

2.3.4 Using Resistivity/Conductivity to Estimate Permeability

Since electrical flow and fluid flow share the same governing equations, it appears possible to use electrical conductivity measurements from wireline to predict hydraulic conductivity. Several studies have confirmed this use of electrical measurements (e.g., Archie, 1950; Jackson et al., 1998; Ball et al., 1997), although most of the reports concern core-scale relationships. The length of the current path through the formation is directly related to the shape, diameter, and sorting of the grains, geometric packing arrangement, and degree of matrix cementation. All of these factors also affect the formation permeability.

Here, we assessed the maximum electrical conductivity (C_{max}) observed in a well to predict that particular well's flow capacity. Core, DST, and production well kh values compared to wireline C_{max} suggest that a useful relationship may exist for the Nisku (Figure 20).

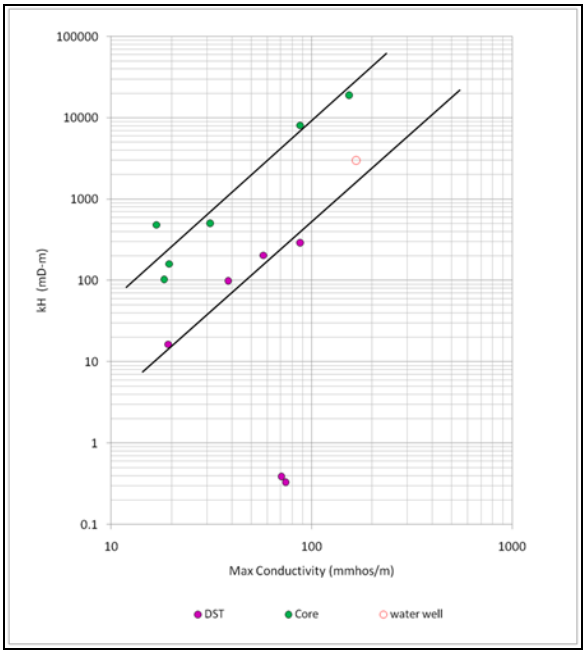

Figure 18: Relationship between maximum conductivity (from wireline logs) and permeability thickness from core (green circles) and DSTs (pink circles). The cause(s) for the two wells with (kh)DST = 0.3 mD-m to have different behaviour

than other wells could not be determined. Open red circle shows water production well (F1/11-29-045-02W5/00) based on known max conductivity measurement and estimate of flow rate.

Core-based kh is larger than the DST and production values (Figure 20) by about a factor of 20. This is reasonable, since we expect locally enhanced permeability seen in core to be limited in lateral extent. The DST and production values will be affected by connectivity beyond the near-wellbore region. The lines of Figure 20 represent speculative C_{max}-kh relationships and have not been tested through either theory or statistical analysis.

From the C_{max}-$(kh)_{prod}$ relationship (lower line of Figure 20), we can estimate flow capacity values, which represent the volumes investigated by DSTs and the production well. A cumulative distribution function of estimated flow capacities can be calculated for every well with useable electrical wirline measurements (Figure 21). For the WASP area, nearly 30% of wells have the potential for greater than 1 D-m, with several wells in two areas possibly having kh > 2 D-m (Figure 22). Simulation studies (see flow simulation chapter for more information) suggest that a minimum of 1 D-m is required for adequate injection capacity. The location of these wells might therefore indicate possible regions within the larger WASP area that would make good injection sites.

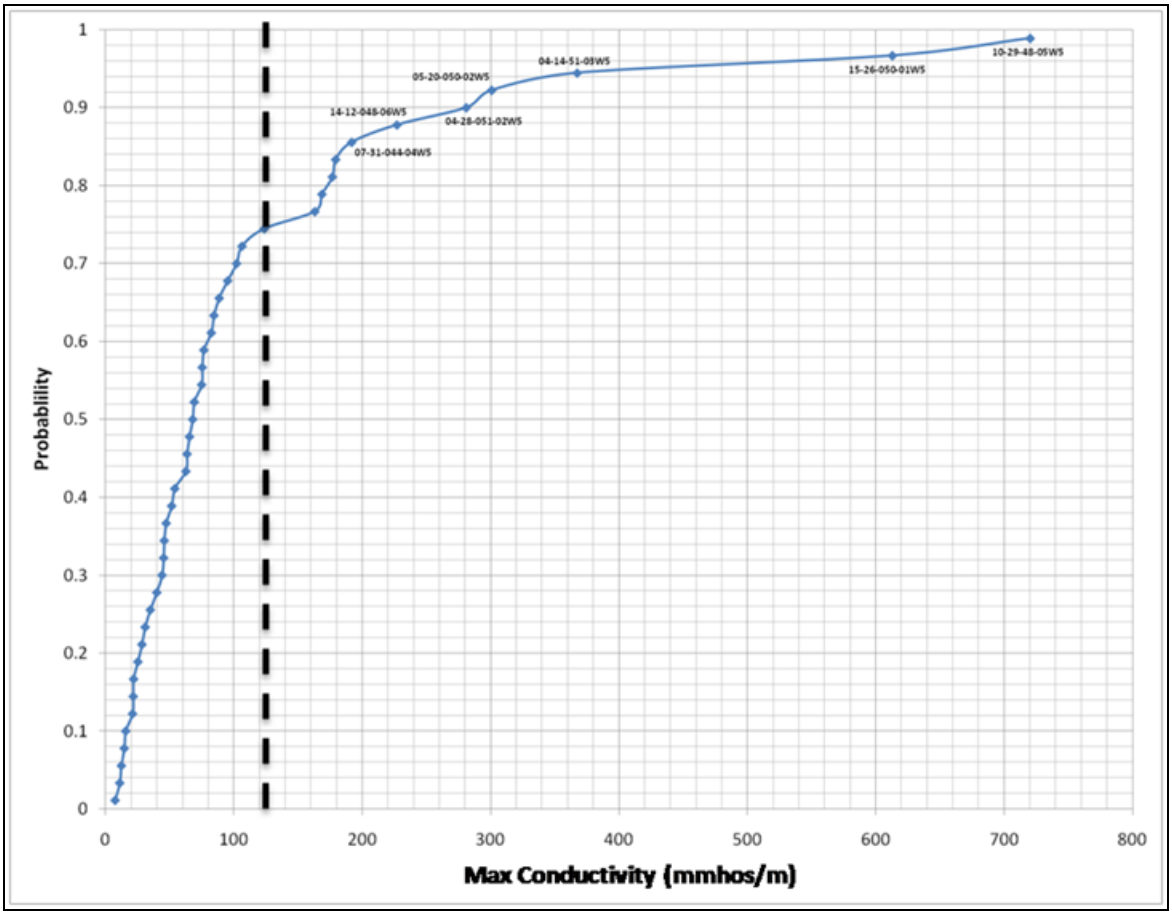

Figure 19: Cumulative distribution function (CDF) of wells based on C_{max} (above). Dashed line indicates the equivalent of a ~1 D-m flow capacity threshold.

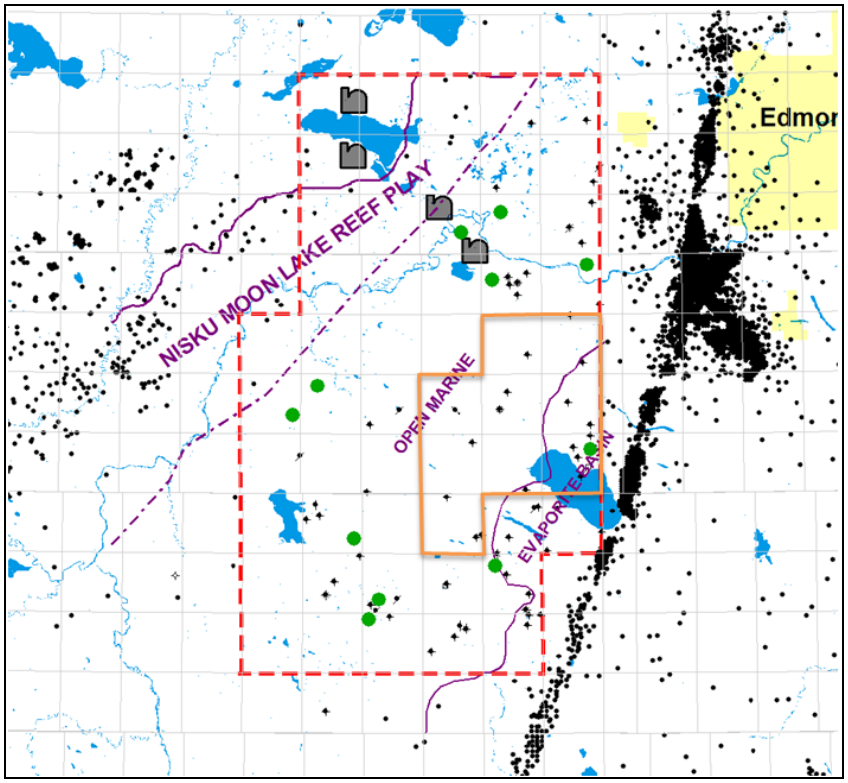

Figure 20: Green circles on map indicate locations of >2 D-m potential flow-capacity wells.

2.3.5 Permeability—Summary

- Wireline resistivity appears to provide a useful flow capacity predictor.
- A minimum electrical conductivity of 150 mhos/m is needed for one Darcy-metre flow capacity to exist for a volume typical of a DST or short-term production test.
- Wireline conductivities suggest that approximately 25% of wells have Darcy-metre flow capacity. These wells are distributed throughout the AOI.
- Two areas in particular show very good flow capacity potential (> 2 Darcy-metres).

2.4 Nisku Lithofacies Distinction

Distinguishing facies within the Nisku carbonate was challenging with very limited core available. The open marine and hypersaline facies were the only two distinctly recognized units (Figure 23), based primarily upon a limited fossil assemblage and presence of more abundant anhydrite in the hypersaline facies. On wireline logs, the distinction between these two facies was difficult to recognize.

A thorough petrophysical analysis of these two facies allows questions important for assessing the suitability for CO_2 injection to be addressed:

1) Is there a quantitative distinction between Nisku open marine and hypersaline facies in wireline log data?
2) Is the hypersaline facies suitable for CO_2 storage?
3) Do wells close to hypersaline/open marine interface show an increased porosity potential?

To address these questions, cumulative distribution functions that aggregate all of the available sonic (Figure 24) and resistivity (Figure 25) data were produced. A significant difference is manifest, with acoustic and resistivity data both suggesting better porosity in the open marine facies. The two facies have a similar abundance of low porosity but, at porosities > 7% (Δt > 53.8 μs/ft), the open marine shows a greater probability of higher-porosity regions. This suggest that the open marine facies has a better prospects as an injection target than the hypersaline facies. While there may be some zones of enhanced porosity in the hypersaline rocks, these are likely to be isolated and have poor connectivity.

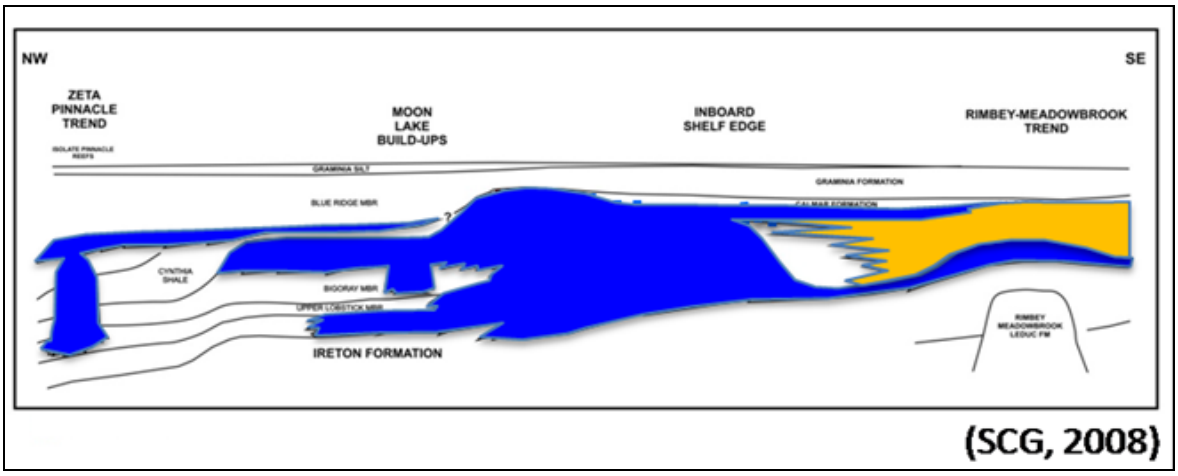

Figure 21: Conceptual model showing distribution of open marine facies (blue) and hypersaline facies (yellow) along an NW-SE cross section of WASP area.

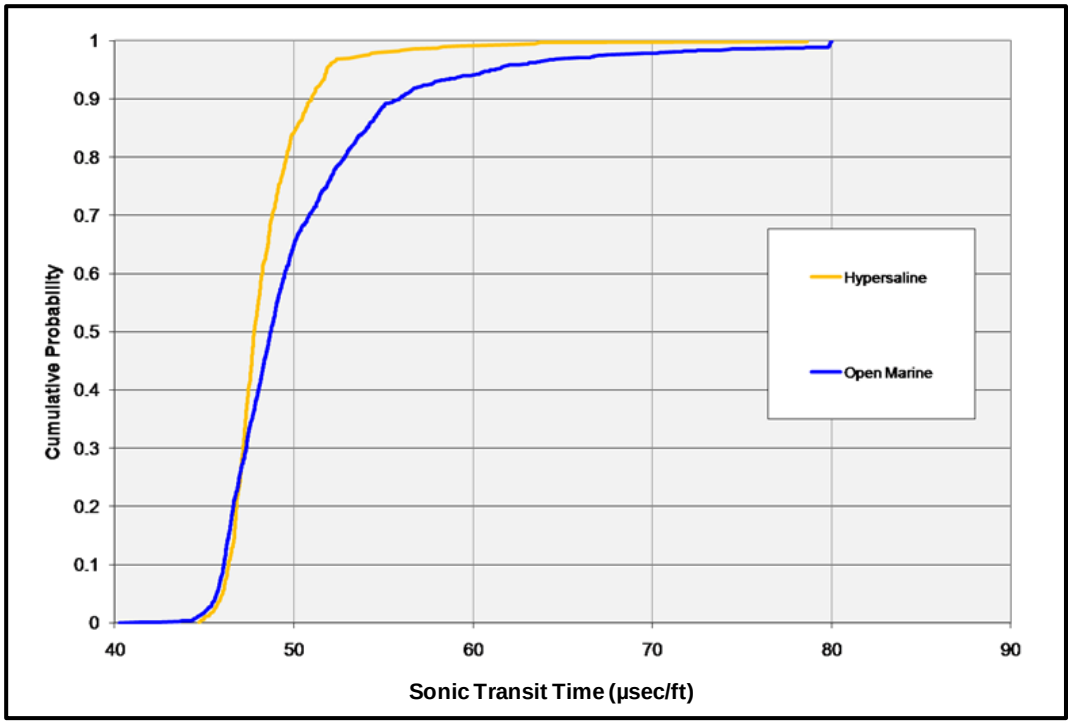

Figure 22: CDF of sonic wireline data for two recognized Nisku facies—open marine (blue) and hypersaline (yellow).

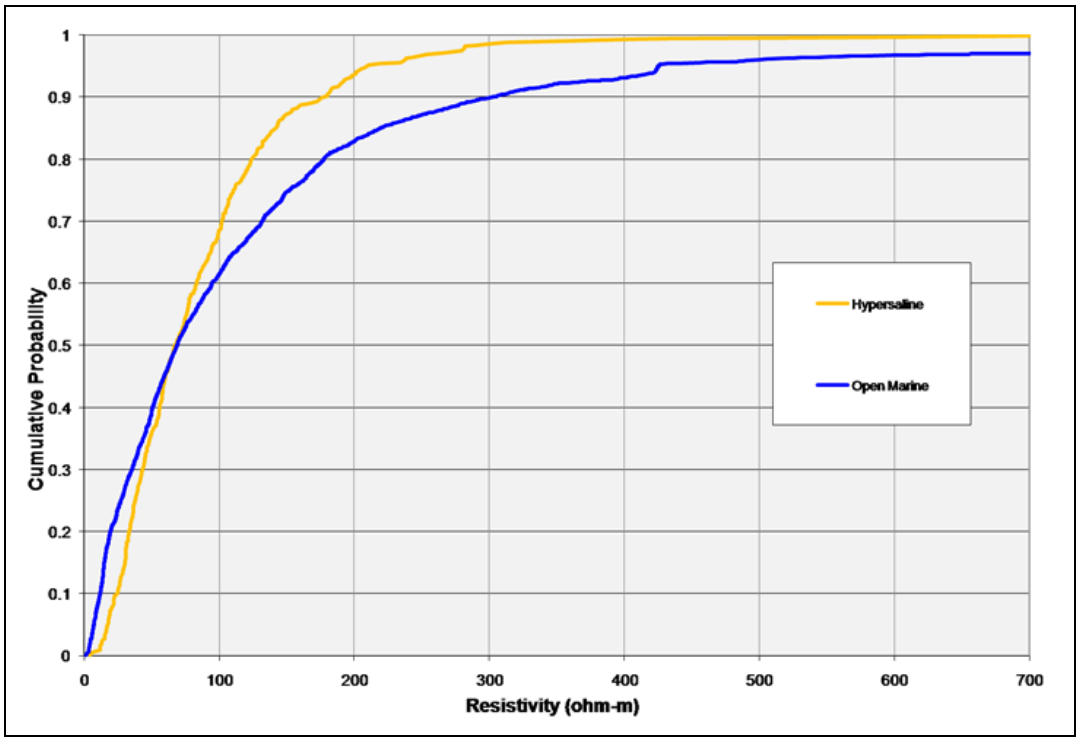

Figure 23: CDF of deep resistivity wireline data for two recognized Nisku facies—open marine (blue) and hypersaline (yellow).

3. GEOMODELLING

Reservoir modelling is necessary to assess the potential capacity of the Nisku aquifer and how fluids will behave during and after CO_2 injection. The reservoir model is an attempt to accurately portray a complex, heterogeneous system using an indirect and incomplete data suite comprising measurements from the forementioned tools. Our main goal is to create accurate models of Nisku aquifer geometry and flow properties consistent with available data and at a scale suitable for the simulation of large-scale fluid injection.

Geostatistics, the statistics and modelling of properties in space and time, provides the estimation techniques that allow the incomplete picture of the potential WASP aquifer to become more complete. Interpretation requiring subjective modelling decisions is critical for capturing the best estimate of geological continuity. While geological detail is usually complex, not all information is necessary for understanding the most significant forces that control subsurface flow.

The workflow for building the Nisku geocelluar model was hierarchical given the variable scales of heterogeneity in the reservoir and the different scales of the data collected. The general sequence was to:

1) Establish horizons and any structural features using wireline log and seismic data in order to build a 3D stratigraphic grid.
2) Construct the depositional grid (i.e., the geostatistical framework).
3) Generate petrophysical models for porosity and permeability using a suite of geostatistical methods.
4) Upscale the geocelluar model (when necessary) and export for reservoir simulation.

When facies property modelling is used, it is also necessary to generate the geometry and distribution of key facies and then populate the facies with petrophysical properties.

The two modelling approaches used for the Nisku characterization were traditional pixel-based methods and object-based (boolean) modelling. Important steps in the workflow will be presented here.

3.1 Structural and Stratigraphic Grid

It is necessary to first establish the reservoir boundary and internal horizons. For the WASP study the boundary was selected based on the region of possible injection and included 54 townships. Formation horizons were identified for approximately 95 wells, and included picks for the tops of the Ireton, Nisku, Calmar, Blue Ridge, Graminia, and Wabamun formations. Additionally, a boundary was established for the Nisku open marine and hypersaline facies, where possible to recognize on wireline geophysical logs. A convergent interpolation method (Taylor series projection with minimum curvature used for smoothing) was used to create the surfaces for the Nisku reservoir envelope (Figure 26). As no major faults were recognized in the zone, the stratigraphy of the reservoir has a simple geometry.

3.2 Depositional Grid

From the stratigraphic grid, a cartesian grid was created for the Nisku reservoir. This grid provides the geostatistical framework for any subsequent property and petrophysical modelling. For this

study the x and y cell dimensions were fixed at 500 m × 500 m (Figure 27) to satisfy computational constraints of modelling the large region of WASP while at the same time providing some reasonable level of geological continuity. All data—well paths, well logs, and seismic data—were conditioned to the cartesian grid once it had been generated. The vertical layering of the grid was set at 30 layers divided unevenly between the 3 zones (Table 2 and Figure 27). The association between the stratigraphic and depositional grid are essentially one to one between each cell.

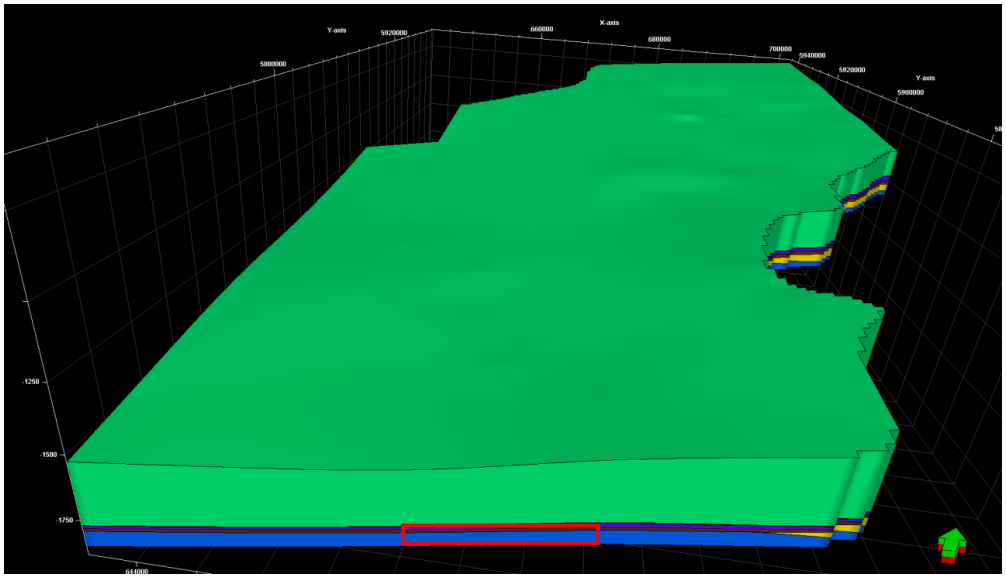

Figure 24: Modelled horizons derived from location of formation tops as identified in well logs. Green—Wabamun (carbonate), Pink—Graminia (shale), Purple—Blue Ridge (carbonate), Brown—Calmar (shale), Blue—Nisku open marine (carbonate), Yellow—Nisku hypersaline (carbonate). Red box shows approximate area of Figure 27 below. Vertical exaggeration = 25.

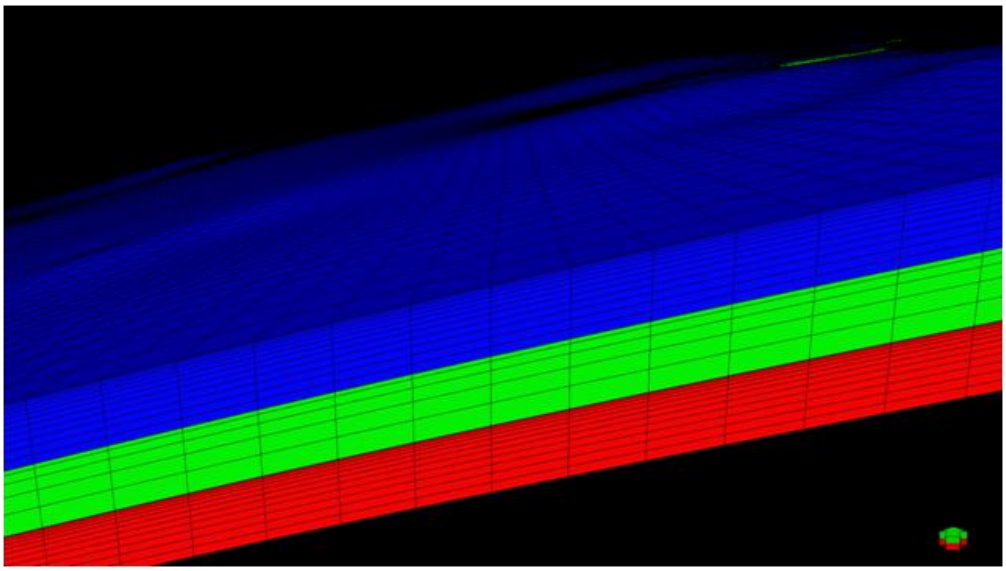

Figure 25: Cross-section of Nisku open marine reservoir model showing vertical and horizontal grid spacing. Note vertical division in 3 zones (blue, green, and red) representing potentially differing flow regimes within reservoir.

Table 2: Vertical grid divisions for Nisku model.

Vertical Layer	Average Thickness (m)	Zone
1–13	1.72	Upper
14–18	4.46	Middle
19–30	1.86	Lower

Vertical grid spacing was designated based upon geological interpretation of wireline logs. As enhanced porosity and permeability zones appear to exist more frequently in the upper and lower thirds of the reservoir, these vertical intervals benefit from a finer vertical resolution when computational constraints are a concern during flow simulation. The upscaling of flow properties is greatly affected by the choice of vertical grid spacing.

3.3 Upscaling Well Logs

Wireline logs were upscaled using an arithmetic average for porosity determination and using a harmonic average for vertical permeability (when appropriate). Logs were treated as lines where each sample value is weighted by a factor proportional to its interval.

3.4 Variogram Analysis

Variogram analysis establishes the geological continuity in porosity and peremeability for the Nisku reservoir. An assumption is made, however, that the nature of these petrophysical properties is homogeneous at some scale. An experimental variogram was calculated and charcteristics interpreted (Figure 28).

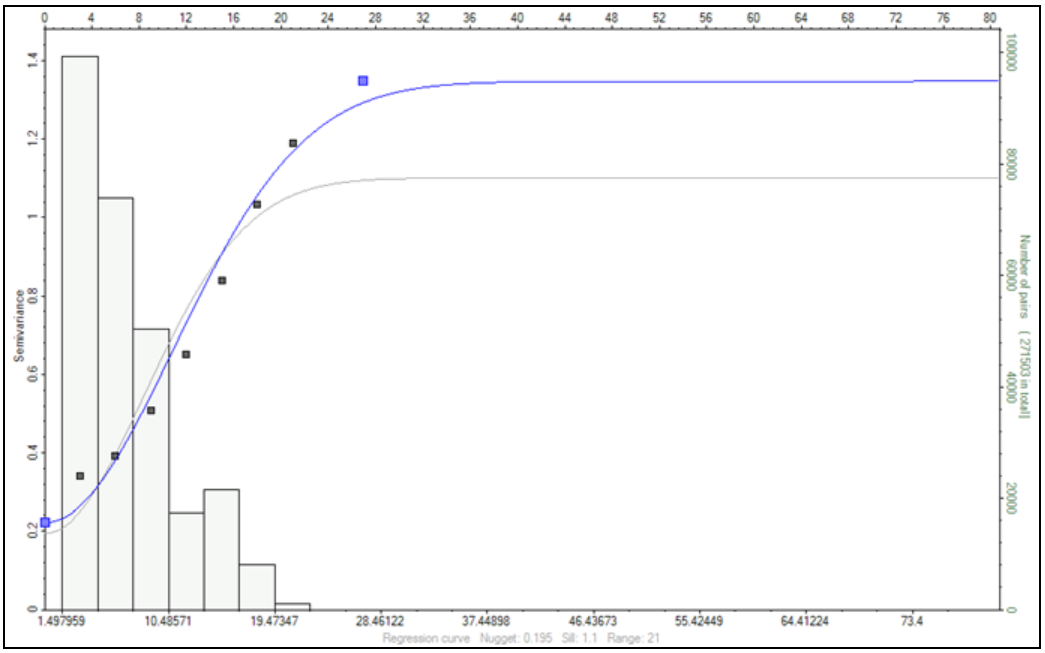

Figure 26: Sample vertical variogram analysis for porosity in the open marine facies of the Nisku reservoir. Vertical range = 27 m, nugget = 0.22. Grey squares show calculated

semivariance at a given correlation distance. Blue line represents experimental variogram (gaussian) that was modelled.

Modelling the variogram allows the ranges and nuggets to be determined, which in turn are critical input parameters for estimation and stochastic simulation. The 3D numerical model is dependent on the specific-variogram algorithm that is selected (Caers, 2005). Here, we used both laterally isotropic (e.g., for kriging) and anisotropic (e.g., for SGS and object-based) semivariograms depending on the modelling objective. Spherical experimental variograms were used for lateral correlation, while gaussian variograms were used in the vertical direction.

3.5 Permeability Estimates

A three-dimensional model of permeability is critical for reservoir characterization and flow simulation. For CO_2 injection, permeability is the most significant variable for controlling total injectivity (see flow simulation section of this report). Data from cores are the typical source of permeability information—which for the WASP study are greatly limited in number and spatial distribution.

A traditional approach for permeability estimation is from porosity using a fitted line (Figure 29) based upon core data. This method has some major drawbacks including poor correlation between porosity and permeability in the data set, few samples from a limited portion of the total Nisku reservoir interval, permeabilities that have the same spatial covariance as porosity, and any existing core permeability data will not be used for populating the static geologic model.

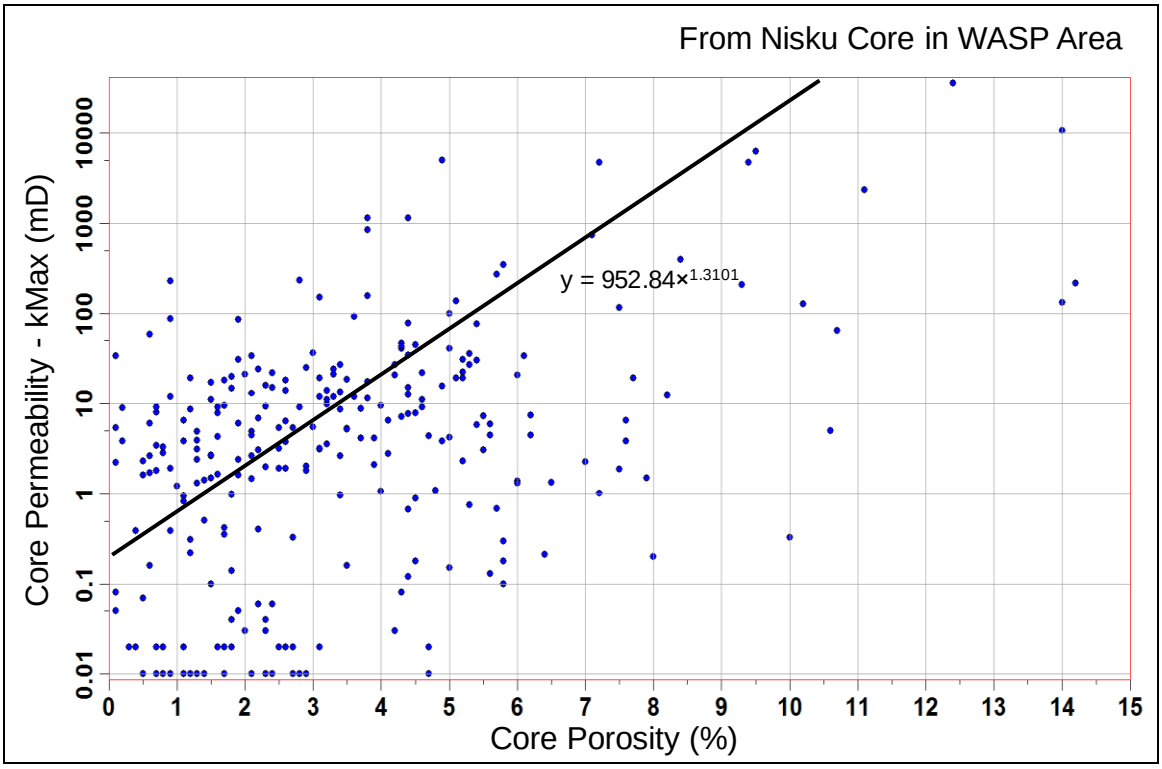

Figure 27: Porosity-permeability cross plot. Manually fitted line (black) manually overestimates permeability when $\phi > 4\%$.

Thus an alternative approach to permeability estimation was employed. Using the maximum conductivity, C_{max}, for an observed interval versus the permeability times thickness (kh) from core and DST data (Figure 20), permeability could be estimated for two scenarios. Using core data, an optimistic scenario:

- $kh = 0.3307 \cdot C_{max}^{2.2268}$

and DST data, a pessimistic scenario:

- $kh = 0.0211 \cdot C_{max}^{2.1973}$

C_{max} was evaluated at the same interval as the vertical grid spacing (h) in order to determine an appropriate permeability value to populate the grid. These values were then used in a conditional simulation (similar to porosity) to create a three-dimensional model of permeability. Porosity was used as the secondary variable in a colocated co-kriging process.

Results from both methods for permeability estimation were used in the flow simulations.

3.6 Pixel-based Modelling

3.6.1 Kriging

A standard geostatistical method for simulating the distribution of porosity and permeability deterministically is to use a kriging algorithm.

Kriging relies on the spatial relationships as described in the variogram for a particular data set. For this technique to be useful, it requires sufficient knowledge of the modelled phenomenon, uncertainty at the unsampled locations to be minimized, and the context of the data to be well understood. These criteria are not, however, well satisfied with the available data for the Nisku in the WASP area.

In the case of the open marine facies for the Nisku, variogram analysis for porosity data from resistivity logs shows the vertical range to be ~14 m, whereas in the horizontal directions the correlations distance were assumed to be large at 5 km. With large interwell distances, it is difficult to assess this.

The result of kriging (Figure 30) does not capture the heterogenity of the system and was not pursued as a viable modelling option. The “bull’s-eye effect”, as areas away from known samples will adopt the mean value for porosity (0.052), is driven by the well locations and is not expected to reflect the true porosity distribution of the reservoir. Also, the heterogeneous nature of reservoir is not captured, for example, we would expect to see regions of enhanced porosity in the interwell regions for this open marine facies.

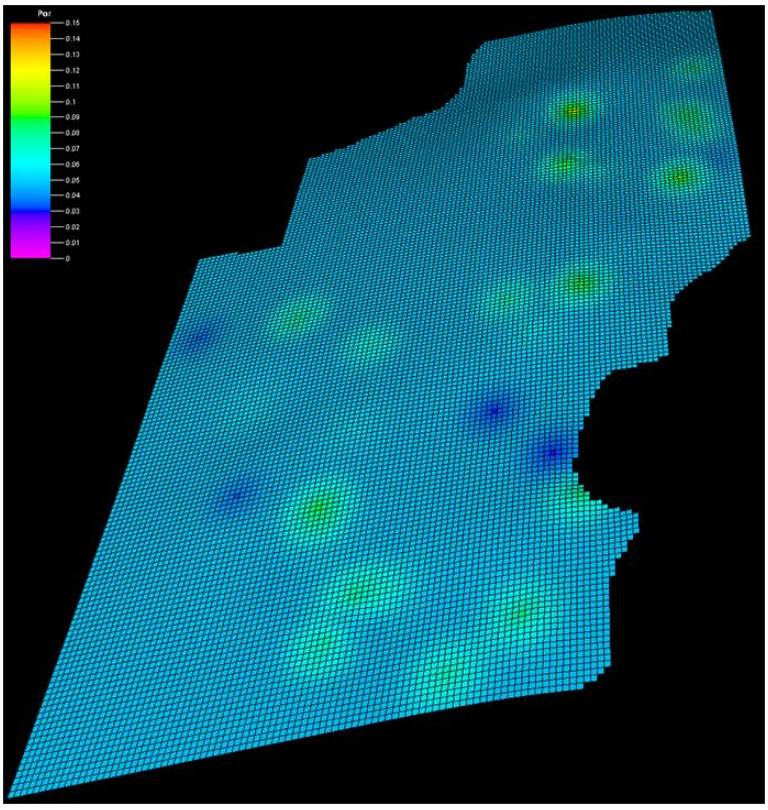

Figure 28: Sample output of ordinary kriging algorithm for porosity of the open marine facies of the Nisku (based on resistivity-derived porosity).

3.6.2 Sequential Gaussian Simulation (SGS)

Another conventional approach is to use a stochastic (probablistic) method which better recognizes uncertainty and incorporates a factor of randomness (Srivastava, 1994). SGS sacrifices some certainty for greater detail. For the WASP area Nisku, this modelling method can provide a more realistic distribution of porosities and permeabilites.

For SGS simulations seismic estimates of acoustic impedance were included as a secondary variable for collocated cokriging (Figure 31). While areally incomplete, the available impedance data were cokriged with a correlation factor of ~0.45 (based on estimates of upscaled cells and normal transform of the data).

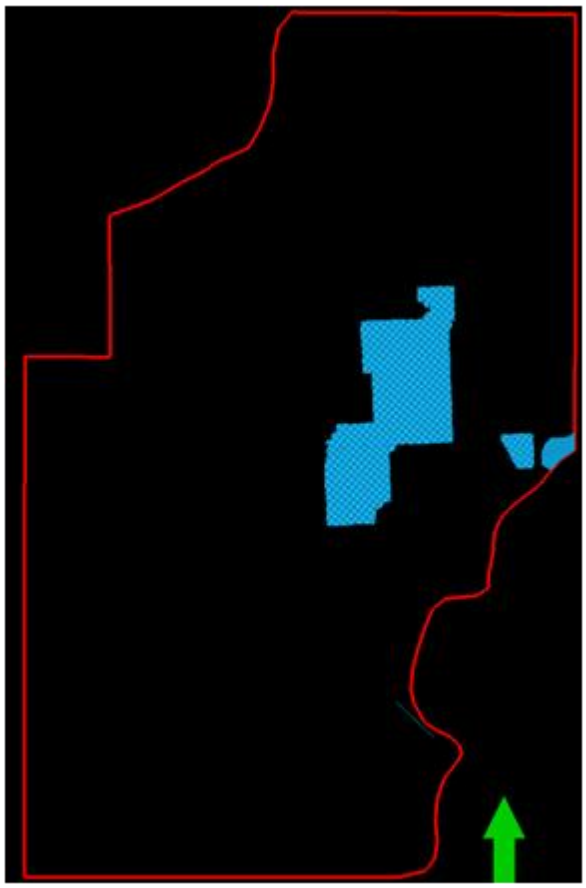

Figure 29: Distribution of available 3D acoustic impedance data used for collocated cokriging.

The semivariogram properties were modelled to be anisotropic:

Range

Major horizontal direction (N 30 E)	8 km
Minor horizontal direction (N 60 W)	5 km
Vertical direction	22 m

Nugget

0.203

A trend (N 30 E) was included to reflect alignment of enhanced porosity regions parallel to the paleo-shoreline during upper Devonian deposition. The major and minor correlation ranges (8 and 5 km) were choosen to be suitably large enough considering the lack of data. The vertical range was dervied from analysis of the vertical variogram.

Of the fifty realizations generated, five were selected for fluid simulation (Figure 32). The porosity and log of permeability results for all realizations have a gaussian distribution. A sample porosity and permeability model is shown in Figure 33. While the realizations developed through SGS methods are qualitatively useful for illustrating potential porosity and permeability distributions in the Nisku open marine facies, quantitatively the constraints for geometries of flow pathways over the entire studied region are poor—a consequence of limited data. Injectivity volumes (as determined through simulation) provide a useable scale-of-magnitude calculation, but there is still a large degree of uncertainty regarding the overall flow connectivity within and between model layers using this method.

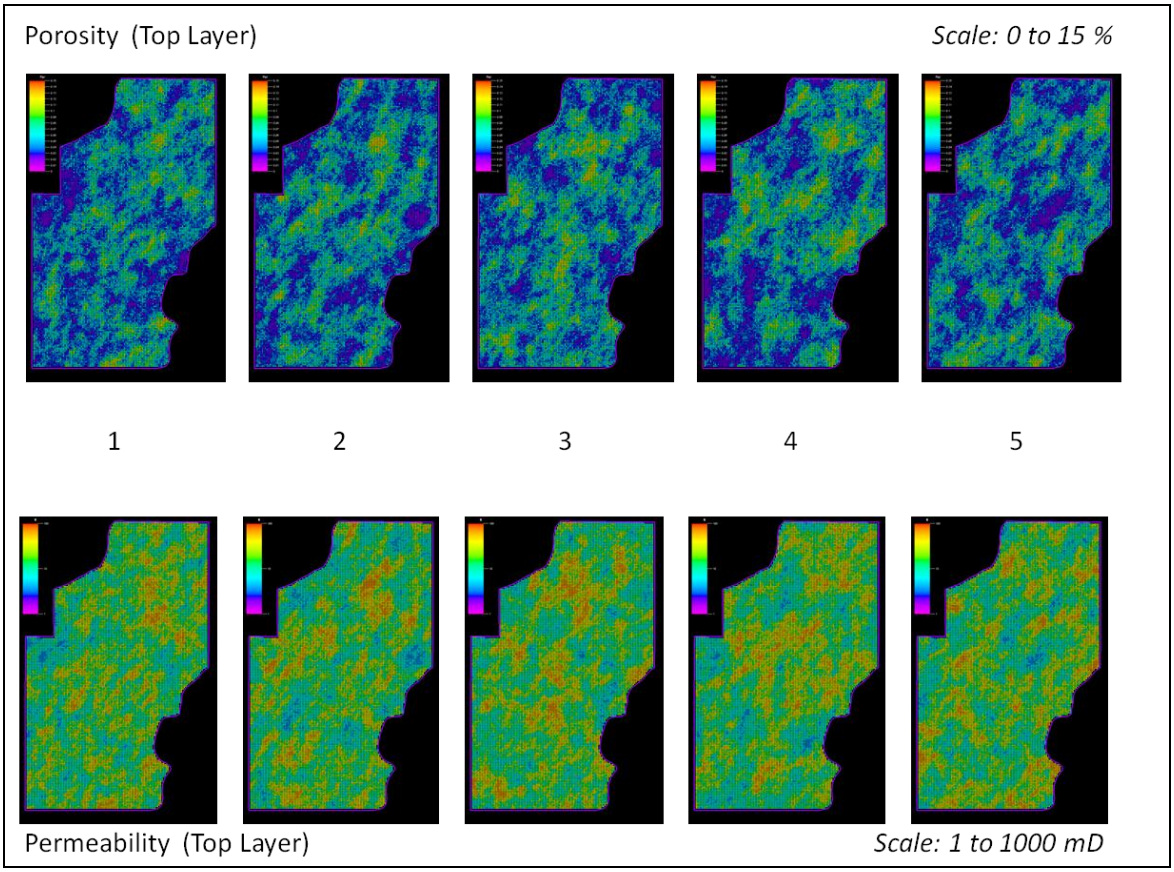

Figure 30: Five SGS realizations for Nisku open marine facies porosity (top) and permeability (bottom).

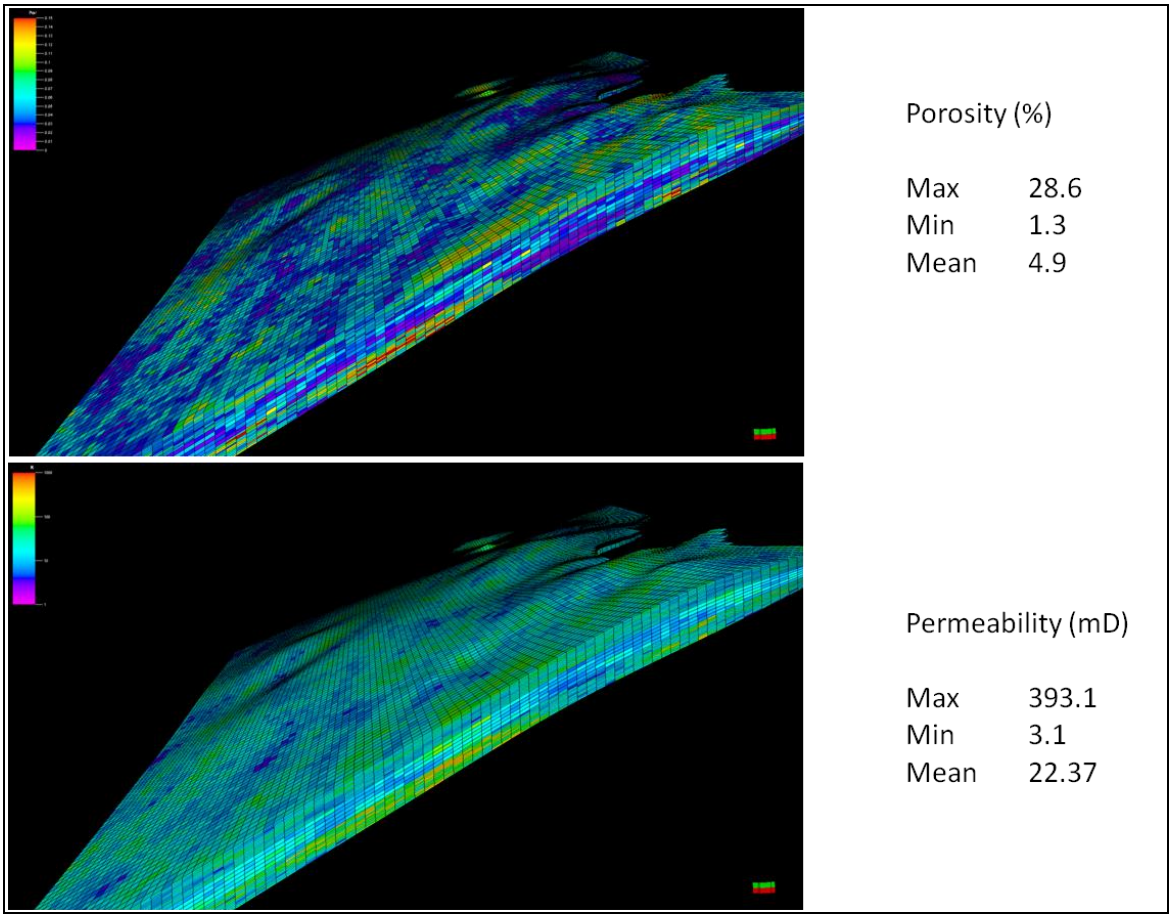

Figure 31: A three-dimensional model realization for porosity and permeability of the Nisku reservoir.

3.7 Object-based Modelling

The distribution and shape of depositional facies in the Nisku carbonate has a critical influence on the hetereogeneity of flow properties. Object-modelling (also known as 'Boolean' modelling) provides a method for incorporating plausible and quantifiable three-dimensional facies geometries into the static earth model. This method can provide more plausible geological shapes than cell-based methods, but it is also more difficult to constrain the models to the actual wireline log and/or seismic data sets (Caers, 2005).

Already in common use for clastic-systems such as fluvial and submarine channels (e.g., Holden et. al, 1998; North, 1996), an objects approach to geomodelling may also have application to carbonate systems—especially in cases where larger reservoir areas are being characterized. The dimensions of facies elements (e.g., reefs, aprons, and shoals), however, need to be quantified in terms of distribution and geometry—thickness, width, aspect ratio, sinuosity, etc. Object parameters may come from outcrop analog studies and/or well-log data (Seifert and Jensen, 2000; North, 1996). To our knowledge, the application of this method has seen limited use for carbonate systems.

The WASP region includes a large area of Nisku carbonate platform deposition. Within that area, a significant challenge is to reasonably quanitfy the shape and density for potential reef systems and

associated facies (i.e., the objects). From a flow-properties perspective, these objects can represent zones of enhanced porosity and permeability. For this study, constraining them to real-world dimensions was done primarily through modern platform analogs that have been mapped via satellite imagery.

3.7.1 Nisku Enhanced Poro-Perm Objects

The nature of reefal build-ups that may occur in areas away from known producing reef-trends is not well known. In trying to predict the density and dimensions of better zones of porosity and permeability throughout the WASP area, a great deal of uncertainty is involved. Studies that include these types of measurements from outcrops or wireline data of the Nisku are rare (e.g., Atchley et al., 2002).

As an alternative approach, modern carbonate facies analogs as classified from satellite imagery may provide some reasonable quantitative constraints (Harris and Kolwalik, 1994; Andrefouet et. al, 2001; Andrefouet et. al, 2003; Bachtel, 2005). This method has been developed primarily during the past decade as higher resolution, multi-spectral remote sensing data have become easier to obtain and process.

For this study, work by Harris and Vlaswinkel (2008) was used to help select values that would be reasonable for carbonate-object geometry and scale. The methods for classifying facies are described in their paper. The analysis provides attribute data for reef associated facied obtained from platform groups based on shape and size (Harris and Vlaswinkel, 2008). Of particular interest are dimensions for partially aggraded reef and apron facies, which were likely to be a common depositional occurrence in the setting of the Nisku platform for the WASP area. Figure 34 shows the workflow for how information from attributes obtained from satellite imagery is used for object modelling.

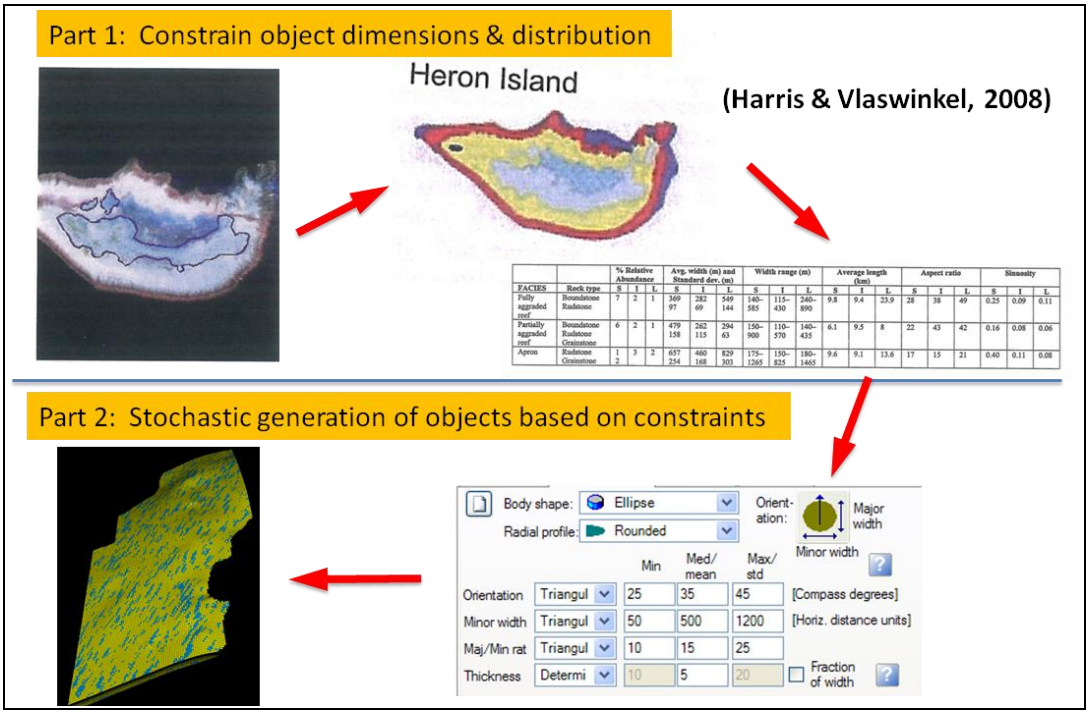

Figure 32: Generalized workflow for facies attributes (as inferred from satellite imagery) of modern carbonate analogs to be used in generating object-based models.

The parameters used for geometry of the objects are shown in Table 3. Lateral distribution of these objects was subjective, based upon conceptual understandings of the Nisku carbonate platform in the WASP study area (see Figures 3 and 35). Two zones, or fairways, were imposed on the model to reflect a greater likelihood of higher porosity and permeability with better connectivity (Figure 35 and Table 4). There is some uncertainty, however, as to the existence of better porosity and permeability along the inboard margin (Figure 35). Appendix 6 discusses this uncertainty.

The vertical distribution of objects was variable depending on the Nisku zone interval being modelled (Figure 27 and Table 4). All objects were populated stochastically in the system, yet still conditioned to existing wireline log data.

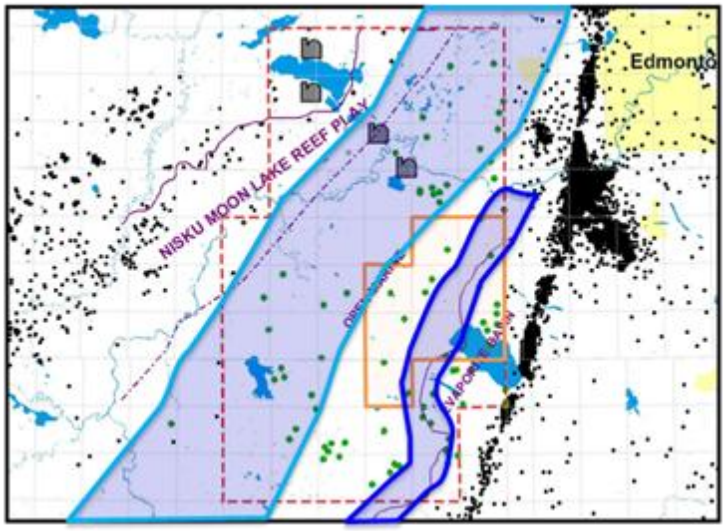

Figure 33: Two regions with higher probability for enhanced porosity and permeability objects based on conceptual modelling of regional deposition. Inboard margin (IBM) (dark blue) and open marine (light blue).

Table 3: Geometry of enhanced porosity and permeability objects. All distributions are triangular between minimum, mean, and maximum.

Enhanced Porosity Class		Minimum (m)	Mean (m)	Maximum (m)
Better	Orientation (Azimuth)	25	35	45
	Major Width	50	500	1200
	Maj/Min Ratio	1	5	7
	Thickness	0.5	5	10
Best	Orientation (Azimuth)	25	35	45
	Major Width	20	300	800
	Maj/Min Ratio	1	5	7
	Thickness	0.1	2	6

Table 4: Division of objects based on vertical interval, enhanced regions, and classes. The percent of total volume objects occupy is a controlled parameter subjectively estimated. IBM = inboard margin, OM = open marine.

Vertical Zone	Enhanced Porosity Object Fairways	Enhanced Porosity Class	% of Total Model Volume
Upper	IBM	Better	3
	IBM	Best	0.5
	OM	Better	7
	OM	Best	1
Middle	IBM	Better	1
	IBM	Best	0.1
	OM	Better	4
	OM	Best	0.5
Lower	IBM	Better	1
	IBM	Best	0.1
	OM	Better	25
	OM	Best	11

Porosities and permeabilities for objects were determined based on the distribution as determined from wireline conductivity (or resistivity) measurements for two classes of enhanced porosity and permeability zones:

1) Better — 8% porosity (normal dist. & 1 std.) and 30 md (log-normal dist & 1 std.)
2) Best — 14% porosity (normal dist. & 1 std.) and 200 md (log-normal dist & 1 std.)

Normal distributions were used for populating object flow properties and SGS modelling was used for baseline carbonate cells. In both cases, modelled flow parameters were constrained to wireline log and seismic-based acoustic impedance data where available.

Several iterations of object distributions were generated (Figure 36), and each was then geostatistically populated with flow properties (Figure 37). The final model outcome was a combination of strong geologic interpretation and traditional geostatistical methods constrained to available data.

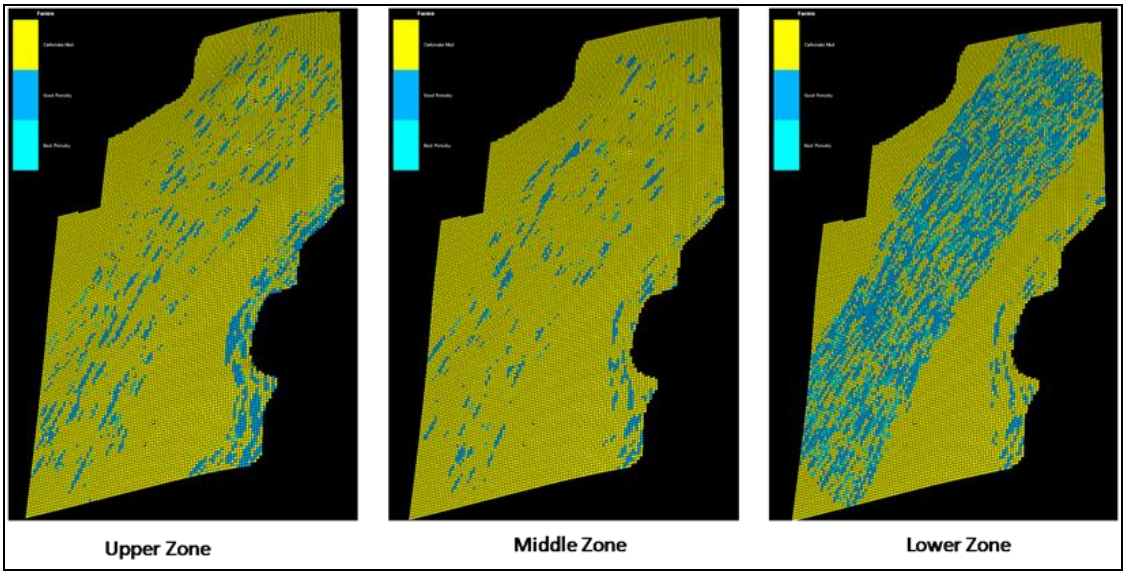

Figure 34: Example of object geometries and distributions for object-based modelling for three Nisku intervals in WASP area. Yellow—background Nisku; blue—better porosity and permeability; turquoise—best porosity and permeability.

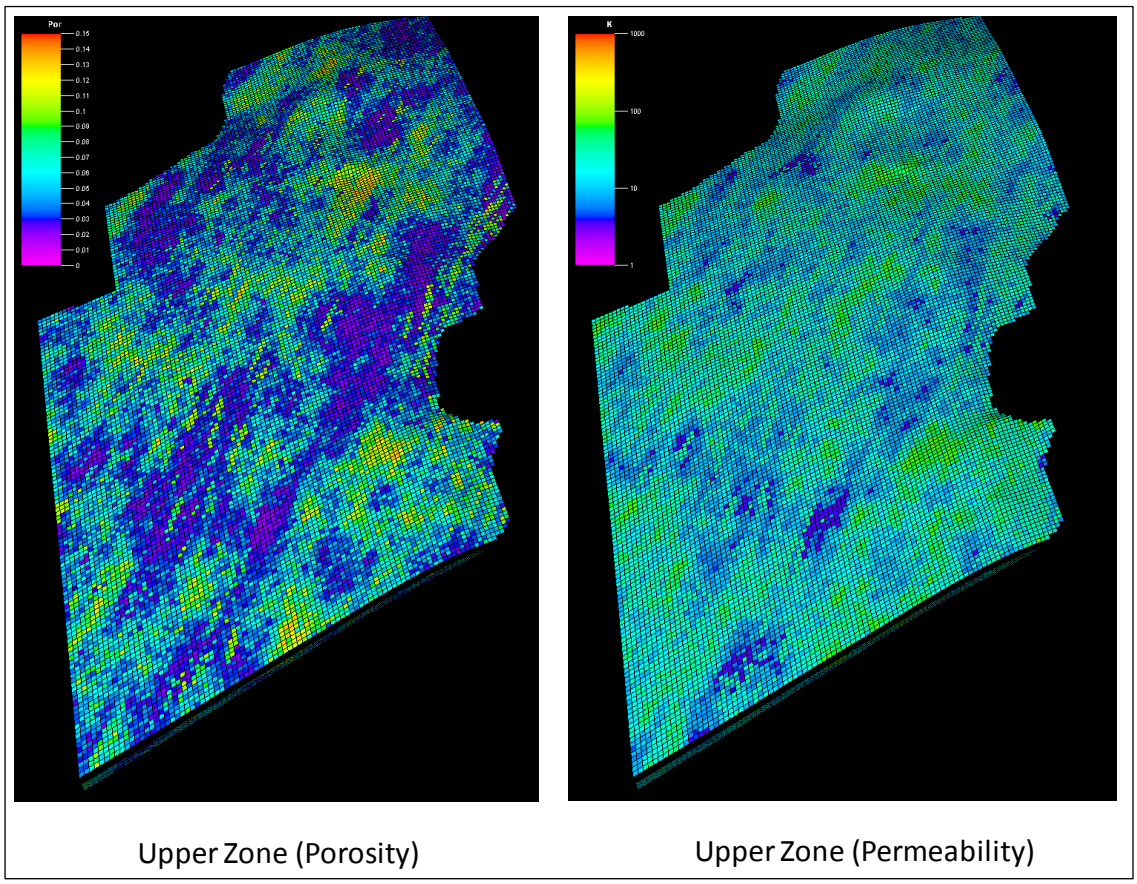

Figure 35: Examples of flow property modelling based on object-models. Porosity (left) scaled 0 to 15% and permeability (right) scaled 1 to 1000 mD.

3.8 Model Validation

Results of both the object- and pixel-based models still require validation. For example, flow simulations of some DSTs could be compared to the field DSTs to assess whether permeability and larger-scale connectivity are adequately captured in the models. Simulation of the water production well could also reveal which models provide the observed deliverabilities along the inboard margin region. Nonetheless, a qualitative inspection suggests a more accurate portrayal of mid-to large-scale reservoir heterogeneity from the object method.

Table 5: Minimum potential storage capacity for Nisku reservoir using WASP boundary. Actual volumes will be larger as aquifer extends to the northwest and southeast of study area. Mean permeability (k) is significantly larger for the object model as isolated grid cells containing high values affect the result.

	Bulk Volume (10^6 m^3)	Pore Volume (10^6 m^3)	Mean ϕ (%)	Mean k (mD)
Homogeneous	305,348	15,267	5.0	30
SGS (50 realizations)	305,348	15,258	4.9	1
Homogeneous	305,348	15,267	5.0	30

3.9 Summary

An accurate representation of the Nisku reservoir is difficult with limited data and measurements. None-the-less, realistic estimates of reservoir capacity and fluid flow behaviour can be made through geomodelling. For the WASP study, probablistic or object-based methods appear to provide the best order-of-magnitude volume approximations (Table 5) and allow variations in connectivity to be examined through fluid simulation. A synthesis of all the model data suggests pore volumes for the Nisku using the WASP boundary will be between 15 and 17 km^3, however the real storage potentail will be much larger as the aquifer extends far to the northeast and southwest of the study area. Qualitatively, the potential flow pathways appear most realistic in an object-based model that allows more geologic interpretation to be included. Further, targeted injection of fluids into the lowest most interval of the Nisku may provide the most benefit. Validation of the models through simulated DSTs are necessary. Further, systematic model sensitivity analysis and subsequent fluid simulation of those models would be useful.

CONCLUSIONS

The available core analyses and petrophysical evaluation of wireline logs indicate mean porosities for the Nisku interval to between 3 and 5%, with localized zones in excess of 10%. Permeability from core measurements shows the median to be 10 mD, but also with recorded values in excess of several Darcys. In trying to map the distribution, size, and connectivity of these better porosity-permeability intervals, wireline logs were used.

Resistivity and conductivity measurements appear to be a useful estimation tool for both ϕ and k. With a known formation resisitivity factor, an assumption of near unity water saturation, and estimates of porosity from core/petrophysical data, the Archie cementation factor was established to be between 2 and 3. Zones with porosity greater than 8% were more often in the lower third of the reservoir interval. Flow capacities, estimated using a relationship between maximum conductivity and permeability thickness from core and DST data, were up to several Darcy-metres in the best cases. The flow capacity is greater than 1 D-m for 25% of the wells with available wireline data

using this method. Connectivity on the reservoir scale is more difficult to evaluate, but production data from wells in nearby hydrocarbon plays suggest 500 mD-m flow capacities.

The goal of geomodelling is to create an accurate representation of the reservoir flow properties for use in fluid injection simulations. To that end, a model framework was created to represent the Nisku reservoir, measured property data were integrated into that framework, and then geostatistical techniques were utilized to populate the model in areas that were unkown. By targeting a deep saline aquifer, reservoir measurements (both direct and indirect) are greatly limited. Deterministic methods are not very useful for modelling a region of this size. Probablistic methods, e.g., SGS, do a better job, but do not capture the heterogeneity as constrained by the conceptual understanding of the depositional history of the Nisku. A less common approach using objects in a Boolean-model workflow allows the target reservoir to be more realistically modelled for connectivity. This method, however, requires the geometry and distribution of higher porosity and permeability zones to be well understood, which for this study was done through a reported analysis of modern analogs mapped with satellite imagery. There still remains a lot of uncertainty as to the nature and extent of high porosity-permeability zones within the targeted injection interval.

The static-earth models were exported for use in fluid-flow simulations (discussed in the flow simulation chapter). The petrophysical analysis and geomodelling suggests potentially good injection volume and flow capacity in the Nisku assuming the best interval and laterally extensive zones are targeted. Seismic data will be invaluable in this process. Another concern is the fracture pressure of the reservoir, which requires detailed geomechanical understanding and a well integrated model of the caprock—in this case the formations of the Winterburn aquitard. The geological model created here can be used as part of this process. Finally, it is necessary to validate the static models for accuracy. This can be done using simulated DSTs and by regenerating models when new data become available.

ACKNOWLEDGEMENTS

We greatly appreciate the financial support of NSERC and AERI, with additional funding from TransAlta, TransCanada, ARC Energy Trust, Penn West Energy Trust, Epcor, Enbridge, ConocoPhillips Canada, Encana, StatOilHydro Canada, Total Canada, Computer Modelling Group, and Golder Associates. We also thank Highpine Oil & Gas for sharing wireline log data and Schlumberger for software access and support. Frank Stoakes and Katrine Foellmer of SCG Ltd. provided invaluable help with geological interpretation and guidance.

REFERENCES

Andrefouet, S., Claereboudt, M., Matsakis, P., Paget, J., and Dufour, P., 2001, Typology of atoll rims in Tuamotu Archipelago (French Polynesia) at landscape scale using SPOT HRV images: Intl. Journal of Remote Sensing, 22, 987–1004.

Andrefouet, S., Kramer, P., Torres-Pulliza, D., Joyce, K.E., Hochberg, E.J., Garza-Perez, R., Mumby, P.J., Riegl, B., Yamano, H., White, W.H., Zubia, M., Brock, J.C., Phinn, S.R., Naseer, A., Hatcher, B.G., and Muller-Karger, F.E., 2003, Multi-site evaluation of IKONOS data for classification of tropical coral reef environments: Remote Sensing of the Environment, 88, 128–143.

Archie, G.E., 1942, The electrical resistivity log as an aid in determining some reservoir characteristics: Am. Inst. Min. Metall. Engineers Transactions, 146, 54–62.

Archie, G.E., 1950, Introduction to petrophysics of reservoir rocks: Bull. Am. Ass. Petrol. Geol., 34, 943–961.

Atchley, S., and McMurray, M., 2002, Devonian (Frasnian) Leduc- and Nisku-equivalent outcrops near Canmore, Alberta: 1-D outcrops as a guide to subsurface stratal architecture: Am. Ass. Petrol. Geol. Annual Conv., Houston, Texas.

Bachtel, S.L., 2005, Platform-scale facies distributions using Landsat data from isolated carbonate platforms: methods to constrain lateral facies continuity for geologic modelling: Am. Ass. Petrol. Geol. Annual Conv., Calgary, Alberta.

Bachu, S., and Bennion, B., 2008, Effects of in-situ conditions on relative permeability characteristics of CO_2-brine systems: Environ Geol, 54, 8, 1707–1722.

Ball, L.D., Corbett, P.W.M., Jensen, J.L., and Lewis, J.J.M, 1997, The role of geology in the behavior and choice of permeability predictors: SPE Formation Evaluation, 12, 1, 32–39.

Caers, J., 2005, Petroleum Geostatistics: Soc. for Petro. Eng., Richardson, Texas, 88 p.

Harris, P.M., and Kolwalik, W.S., eds., 1994, Satellite Images of Carbonate Depositional Settings: Examples of Reservoir- and Exploration-scale Geologic Facies Variation: Am. Ass. Petrol. Geol., Methods in Exploration Series, 11, 147 p.

Harris, P.M., and Vlaswinkel, B., 2008, Modern isolated carbonate platforms: Templates for quantifying facies attributes of hydrocarbon reservoirs: Soc. for Sed. Geol. Special Pub., 89, 323–341.

Hitchon, B., 1996, Aquifer Disposal of Carbon Dioxide: Geoscience Publishing Ltd., Sherwood Park, Alberta, 165 p.

Holden, L., Hauge, R., Skare, O., and Skorstad, A., 1998, Modelling fluid reservoirs with object models: Mathematical Geology, 30, 5, 473–496.

Michael, K., Bachu, S., Buschkuehle, B.E., Haug, K., Grobe, M., and Lytviak, A.T., 2006, Comprehensive characterization of a potential site for CO_2 geological storage in central Alberta, Canada: Proceedings, CO_2SC Symposium, Berkeley, California, 4 p.

Michael, K., Bachu, S., Buschkuehle, B.E., Haug, K., and Talman, S., 2009, Comprehensive characterization of a potential site for CO_2 geological storage in central Alberta, Canada: Carbon

Dioxide Sequestration in Geological Media – State of the Art (M. Grobe, J. Pashin and R. Dodge, eds.), AAPG Studies in Geology 59, 227–240.

North, C.P., 1996, The prediction and modelling of subsurface fluvial stratigraphy *in* Advances in Fluvial Dynamics and Stratigraphy, P.A. Carling and M.R. Dawson (eds.): John Wiley & Sons, New York, 395–508.

Jackson, P.D., Harvey, P.K., Lovell, M.A., Gunn, D.A., Williams, C.G., and Flint, R.C., 1998, Measurement scale and formation heterogeneity: effects on the integration of resistivity data: Geological Society Special Publication, 136, 261–272.

Lucia, J.F., 2007, Carbonate Reservoir Characterization: An Integrated Approach: Springer, Berlin, 336 p.

SCG Ltd., Stoakes Consulting Group, 2009, personal communication.

Seifert, D. and Jensen, J.L., 2000, Object and pixel-based reservoir modelling of a braided fluvial reservoir: Mathematical Geology, 32, 5, 581–603.

Srivastava, R.M., 1994, An overview of stochastic methods for reservoir characterization in AAPG Computer Applications in Geology No. 3, Stochastic Modelling and Geostatistics: Principles, Methods and Case Studies, J.M. Yarus and R.L. Chambers (eds): American Association of Petroleum Geologists, Tulsa, OK, 3–16.

Switzer, S.B., Holland W.G., Christie, D.S., Graf, G.C., Hedinger, A.S., McAuley, R.J., Wierzbicki, R.A., and Packard, J.J., 1994, Devonian Woodbend - Winterburn strata of the Western Canada Sedimentary Basin *in* Geological Atlas of the Western Canada Sedimentary Basin, G.D. Mossop and I. Shetsen (comp.): Canadian Society of Petroleum Geologists and Alberta Research Council, Special Report 4.

Wright, G.N., McMechan M.E., and Potter, D.E.G., 1994, Structure and architecture of the Western Canada Sedimentary Basin *in* Geological Atlas of the Western Canada Sedimentary Basin, G.D. Mossop and I. Shetsen (comp.): Canadian Society of Petroleum Geologists and Alberta Research Council, Special Report 4.

Wylie, M. R., Gregory, A. R, and, Gardner, L. W., 1956, Elastic wave velocities in heterogeneous and porous media: Geophysics, 21, 41–70.

APPENDIX 1: WELLS (NISKU)

UWI	Drilling Completed	TVD (m)	Formation@TD	BH Temp. (°C)	Core	Canstrat
100/03-16-043-05W5/00	06/07/1954	3080.3	Dbvrh_lk	?	Y	
100/14-26-044-02W5/00	11/28/1985	2630	Dbvrhl_lk	74		
100/15-35-044-02W5/00	02/16/1988	2938	Cdeadwood	76		Y
100/16-36-044-02W5/00	01/19/1991	2600	Dbvrhl_lk	70		
100/01-18-044-03W5/00	04/14/1985	2792	Dbvrhl_lk	59		Y
100/12-22-044-03W5/00	05/05/1953	2659.4	Dduvernay	73		Y
100/06-26-044-03W5/00	08/08/1978	2412	Dnisku	71		
100/10-27-044-03W5/00	11/23/1977	2420.1	Direton	69		
100/07-31-044-04W5/00	10/03/1974	2631.9	Direton	67	Y	
100/10-33-044-04W5/00	04/07/1975	2578.6	Direton	46		
100/06-02-045-02W5/00	11/10/1977	2779.8	Delk_pt	78		Y
100/15-11-045-02W5/00	02/16/1954	2596.9	Dduvernay	79		Y
100/14-21-045-02W5/00	08/26/1960	2580.4	Dbvrhl_lk	71		Y
1F1/11-29-045-02W5/00	11/27/2002	2321	Direton	?		
100/14-32-045-02W5/00	07/13/1997	2632	Direton	66		
100/14-16-045-03W5/00	01/14/2006	2443	Direton	?		
100/06-05-045-04W5/00	02/13/1975	2592.3	Direton	66		
102/16-06-045-04W5/00	08/06/1975	2947.4	Dbvrhl_lk	72		
100/07-08-045-04W5/00	03/17/1976	2567.9	Dnisku	69	Y	Y
100/06-10-045-04W5/00	12/28/1985	2510	Dnisku	64		
100/14-09-045-05W5/00	08/20/1997	3100	Dbvrhl_lk	93		
100/04-22-045-05W5/00	08/05/1954	3159.3	Delk_pt	93	Y	Y
100/10-36-045-05W5/00	02/05/1976	2514.6	Direton	73	Y	
100/11-24-045-08W5/00	08/25/1978	3150	Dbvrhl_lk	?	Y	
100/01-01-046-01W5/00	08/10/1983	2258.8	Dleduc	68		
100/02-01-046-01W5/00	11/07/1987	2284	Dleduc	66		
100/09-01-046-01W5/00	02/12/1972	2272.9	Dleduc	85		
104/06-06-046-01W5/00	08/21/2004	2484	Direton	72		
100/01-13-046-01W5/00	03/26/1953	2283	Dcook_lk	69		Y
100/06-29-046-01W5/00	10/09/1984	2460	Dbvrhl_lk	68		
100/10-09-046-02W5/00	01/28/1966	2790.7	Delk_pt	87		Y
100/10-25-046-02W5/00	07/30/1966	2690.2	Delk_pt	64		Y
102/12-25-046-02W5/00	06/21/1996	2545	Dbvrhl_lk	81		
100/11-12-046-03W5/00	02/10/1953	2560	Direton	71		
100/16-12-046-03W5/00	01/02/1948	2746.6	Dduvernay	76	Y	Y
100/11-33-046-03W5/00	01/15/1953	2564.9	Dduvernay	74	Y	Y
100/05-12-046-05W5/00	06/13/1978	2481	Direton	76	Y	Y
100/06-19-046-05W5/00	09/11/1958	2865.1	Dbvrhl_lk	85	Y	Y
100/10-20-046-05W5/00	10/29/1978	2565	Dwoodbend	75		
100/14-29-046-05W5/00	06/26/1993	2515	Direton	79		
100/09-10-047-01W5/00	04/17/1987	2311.5	Direton	71		
100/10-22-047-01W5/00	09/23/1964	2539	Dbvrhl_lk	72		Y

UWI	Drilling Completed	TVD (m)	Formation@TD	BH Temp. (°C)	Core	Canstrat
100/08-26-047-01W5/00	10/08/1973	2362.2	Dbvrhl_lk	71		
100/12-27-047-01W5/00	01/02/1965	2401.8	Dbvrhl_lk	63		
100/16-35-047-01W5/00	06/18/1973	2293.6	Dbvrhl_lk	74		
100/06-02-047-02W5/00	07/16/1961	2516.1	Dbvrhl_lk	80		Y
100/04-36-047-03W5/00	04/26/1949	2562.8	Dcook_lk	77	Y	Y
100/02-06-047-04W5/00	02/21/1955	3092.2	Cdeadwood	104	Y	Y
100/09-24-047-06W5/00	09/21/1991	2723	Dduvernay	69		
100/16-02-048-01W5/00	10/31/1952	2286	Dduvernay	62	Y	Y
100/02-21-048-01W5/00	02/12/1962	2286	Dbvrhl_lk	61		Y
100/08-17-048-02W5/00	10/17/1984	2050	Dnisku	69		
100/02-28-048-02W5/00	01/17/1955	2348.2	Direton	68		Y
100/06-15-048-03W5/00	09/14/1959	2674.6	Dgilwood	67		
100/16-06-048-04W5/00	08/18/1959	2874.3	Cambrian	71		
100/08-15-048-04W5/00	05/07/1956	2560	Dbvrhl_lk	71		Y
100/10-29-048-05W5/00	07/14/1979	2355	Direton	80		
102/14-12-048-06W5/00	04/04/1989	2414	Direton	70		
100/14-29-048-06W5/00	05/27/1954	3146.1	Cambrian	76	Y	Y
100/04-11-049-01W5/00	11/12/1950	2128.7	Dduvernay	62		
100/16-33-049-01W5/00	02/22/1954	2102.5	Dcook_lk	41		
100/15-11-049-02W5/00	08/13/1950	2263.1	Dduvernay	76		Y
100/07-33-049-06W5/00	04/18/1978	2322.6	Direton	72		
100/16-01-050-01W5/00	07/06/1952	2083.6	Dduvernay	82		
100/15-26-050-01W5/00	09/06/1949	1981.2	Dduvernay	54		
100/15-10-050-02W5/00	02/09/1948	2040.6	Direton	71	Y	
100/16-16-050-02W5/00	12/02/1960	2295.1	Dbvrhl_lk	63		
100/04-20-050-02W5/00	12/21/1958	1942.2	Direton	56		
100/05-20-050-02W5/00	09/09/1965	2247.6	Dbvrhl_lk	61		
100/10-21-050-02W5/00	08/19/1997	1900	Direton	64		
100/02-22-050-02W5/00	02/26/1955	2581	Dbvrhl_lk	46		Y
100/02-26-050-02W5/00	08/13/1954	2243.3	Dbvrhl_lk	63		Y
100/04-11-051-01W5/00	04/11/1950	2042.8	Dduvernay	?	Y	Y
100/09-16-051-01W5/00	10/04/1954	2088.5	Dduvernay	61	Y	
100/04-36-051-01W5/00	05/01/1948	2128.7	Dcook_lk	?	Y	
100/04-28-051-02W5/00	03/11/1950	2183.6	Dcook_lk	57		Y
100/04-14-051-03W5/00	07/23/1963	1905	Direton	56		
100/05-08-051-04W5/00	06/24/1978	2077	Direton	59	Y	
100/04-14-051-04W5/00	06/24/1978	2057.4	Direton	55	Y	
100/01-34-051-04W5/00	11/09/1978	2060	Direton	54		
100/02-29-051-05W5/00	03/24/1994	2128	Dnisku	50	Y	
100/03-12-052-01W5/00	09/02/1981	2072	Dbvrhl_lk	60		
100/09-13-052-01W5/00	07/20/1949	1830	Direton	64		
100/10-05-052-02W5/00	01/08/1968	2920	preCamb	76		Y
100/04-34-052-03W5/00	02/07/1952	2103.1	Dduvernay	51	Y	
100/11-34-052-03W5/00	01/11/1998	1815	Dnisku	46		
100/15-23-052-04W5/00	02/15/1982	1960	Direton	47	Y	Y
100/05-01-052-05W5/00	08/26/1973	2133.6	Direton	57	Y	Y

UWI	Drilling Completed	TVD (m)	Formation@TD	BH Temp. (˚C)	Core	Canstrat
100/16-18-052-05W5/00	05/26/1956	2797.1	Delk_pt	74	Y	Y
100/08-30-052-05W5/00	09/17/1984	2714	Cambrian	65		
100/04-31-052-05W5/00	09/24/1978	2090	Direton	70	Y	
100/07-11-053-01W5/00	08/08/1949	1966.3	Dduvernay	59	Y	
100/04-12-053-02W5/00	11/28/1950	1981.2	Dduvernay	60	Y	Y
100/10-10-053-03W5/00	02/25/1974	1956.8	Direton	53	Y	
100/10-14-053-03W5/00	01/15/1976	1876	Direton	53		
100/07-33-053-03W5/00	10/31/1961	1868.4	Direton	46		
100/13-36-053-03W5/00	07/05/1978	1853.2	Direton	50	Y	
100/13-36-053-05W5/00	06/11/1949	2067.8	Direton	63		

Table Legend

Blue	Wells out of WASP study area
Yellow	Wells in Moon Lake play

Formation abbreviations

Cambrian	→	Cambrian
Cdeadwood	→	Deadwood
Dbvrh_lk	→	Beaverhill Lake
Dcook_lk	→	Cooking Lake
Dduvernay	→	Duvernay
Delk_pt	→	Elk Point
Dgilwood	→	Gilwood
Direton	→	Ireton
Dleduc	→	Leduc
Dnisku	→	Nisku
Dwoodbend	→	Woodbend
PreCamb	→	Pre-Cambrian

APPENDIX 2: WELL CORES (WASP AREA)

CPA Format Well ID	Date Drilling Completed	Core Analysis	Logged	Reported Depth Interval (ft)	Total Core (ft)	ERCB
100/07-31-044-04W5/00	10/03/1974	Y	Y	8497–8516	19	5B/4"/W
100/07-08-045-04W5/00	03/17/1976	Y	Y	8215–8275	58	16B/4"/W
100/04-22-045-05W5/00	08/05/1954	Y (new)	Y	8460–8594	194	27B/3"/W
100/10-36-045-05W5/00	02/05/1976	Y	Y	7933–7983	50	28B/4"/W
100/16-12-046-03W5/00	01/02/1948	N	Y	7319–7339 and 7408–7419	31	2B/2"/W
100/11-33-046-03W5/00	01/15/1953	Y (new)	Y	7215–7351	136	27B/3"/A
100/05-12-046-05W5/00	06/13/1978	Y	Y	7831–7891	60	13B/3"/R
100/06-19-046-05W5/00	09/11/1958	Y	Y	8054–8078	24	5B/3"/R
100/06-02-047-02W5/00	07/16/1961	Y (new)	Y	6841–6876 and 6908–6921	48	7B/3"/W, 3B/3"/W
100/04-36-047-03W5/00	04/26/1949	N	Y	6990–7034	44	1B/1"/W
100/02-06-047-04W5/00	02/21/1955	Y (new)	Y	7642–7753	111	24B/3"/R
100/16-02-048-01W5/00	10/31/1952	Y (new)	Y	6120–6135 and 6137–6186	34	13B/3"/W
100/15-11-049-02W5/00	08/13/1950	Y (new)	Y	6129–6155 and 6260–6278	44	6B/3"/W, 4B/3"/W
100/15-10-050-02W5/00	02/09/1948	N	Y	6040–6094	54	3B/1"/W
Outside Study Area						
100/03-16-043-05W5/00	06/07/1954	Y (new)	Y	8878-8974	96	18B/3"/W
100/11-24-045-08W5/00	08/21/1978	Y (new)	Y	8965-9012	47	10B/3"/W

Notes

1. Complete core analysis data available in WASP project archives.
2. Whole core photos available for the following wells:
    - 100/04-22-045-05W5/00
    - 100/16-02-048-01W5/00
    - 100/15-11-049-02W5/00

APPENDIX 3: WIRELINE GEOPHYSICAL LOGS

UWI	Wireline Geophysical Logs
100/14-26-044-02W5/00	S (295.8 ~ 2618.3m);DILL (1780.0 ~ 2628.1m);FLUID L (281.0 ~ 2630.0m)
100/15-35-044-02W5/00	S (1400.0 ~ 2584.0m);CS (450.0 ~ 2580.0m);CN-LD (875.0 ~ 2590.0m);DIL (450.0 ~ 2591.0m);C-VOL (450.0 ~ 2590.0m);HR-DIP (2150.0 ~ 2600.0m);SWF (1400.0 ~ 2584.0m);FT (2150.0 ~ 2584.0m);BHTV (2189.1 ~ 2236.0m);CP (430.0 ~ 2938.0m);CS (2575.0 ~ 2920.0m);CN-LD (2575.0 ~ 2933.0m);DIL (2575.0 ~ 2932.0m)
100/16-36-044-02W5/00	S (403.9 ~ 2596.8m);CNFD (1600.0 ~ 2600.0m);DILL (403.9 ~ 2598.6m);CP (390.0 ~ 2219.0m)
100/01-18-044-03W5/00	CS (327.0 ~ 2778.0m);CN-LD (413.3 ~ 2790.8m);DISF (413.3 ~ 2790.3m);C-VOL (413.0 ~ 2780.0m);FLUID L (2730.0 ~ 2792.0m);FLUID L (398.0 ~ 2792.0m)
100/12-22-044-03W5/00	ES (180.4 ~ 2659.4m);LL (180.4 ~ 2659.4m)
100/06-26-044-03W5/00	SONIC (260.0 ~ 2410.0m);DIL (260.0 ~ 2411.0m);PERF (1850.0 ~ 2000.0m);ND-LITH (260.0 ~ 2412.0m)
100/10-27-044-03W5/00	SONIC (248.4 ~ 2415.8m);DIL (248.4 ~ 2415.8m);CB (1524.0 ~ 1975.1m);COLLAR (1850.0 ~ 1890.0m);TRACE L (1825.0 ~ 1905.0m);ND-LITH (248.4 ~ 2417.1m)
100/07-31-044-04W5/00	SONIC (265.2 ~ 2627.1m);DIL (265.2 ~ 2628.3m);GR-CORR (2000.0 ~ 2143.0m);ND-LITH (1066.8 ~ 2629.8m)
100/10-33-044-04W5/00	SONIC (271.3 ~ 2578.6m);DIL (271.3 ~ 2578.0m);ND-LITH (2042.2 ~ 2578.6m)
100/06-02-045-02W5/00	SONIC (1676.4 ~ 2779.2m);NEUT (457.2 ~ 2286.0m);DIL (461.8 ~ 2778.6m);CB (1676.4 ~ 1995.2m);GR (1714.2 ~ 1791.8m);PERF (1801.4 ~ 1856.2m);IND-LOG (1767.0 ~ 1804.0m);ND-LITH (461.8 ~ 2779.8m);GR (1730.0 ~ 1789.7m)
100/15-11-045-02W5/00	ES (188.1 ~ 1430.4m);ML (655.3 ~ 1429.5m);ES (1430.4 ~ 2596.0m);ML (1798.3 ~ 2286.0m)
100/14-21-045-02W5/00	IE (274.3 ~ 2576.2m);ML (670.6 ~ 2578.0m);SONIC (274.3 ~ 2574.3m)
1F1/11-29-045-02W5/00	
100/14-32-045-02W5/00	CS (329.0 ~ 2457.0m);CN-LD (329.0 ~ 2470.0m);GRN-COL (1696.0 ~ 2618.1m);DIL (329.0 ~ 2472.5m);GR-CORR (1550.0 ~ 1700.0m);COLLAR (1783.0 ~ 1840.0m);MUD-HYD (1765.0 ~ 2625.0m);GR-CORR (1800.0 ~ 1855.0m);COLLAR (1796.0 ~ 1866.0m);MUD-HYD (1840.0 ~ 2645.0m);GR-CORR (1600.0 ~ 1866.0m);COLLAR (1837.0 ~ 1840.0m);COLLAR (1764.4 ~ 1836.3m);COLLAR (1772.6 ~ 1842.0m);COLLAR (1642.8 ~ 1699.9m)
100/14-16-045-03W5/00	ML (2368.5 ~ 2484.0m);CS (456.0 ~ 815.0m);D-S-S-I (2368.5 ~ 2473.0m);CN-LD (2368.5 ~ 2492.5m);C-VOL (456.0 ~ 815.0m);ML (2324.0 ~ 2430.0m);CN-LD (2324.0 ~ 2437.0m);DIL (2324.0 ~ 2439.6m)
100/06-05-045-04W5/00	SONIC (265.2 ~ 2590.8m);GRN-COL (1825.0 ~ 2165.0m);DIL (267.3 ~ 2584.4m);CB (2450.0 ~ 2568.0m);GR-CORR (2040.0 ~ 2100.0m);PERF (2510.0 ~ 2550.0m);COLLAR (2475.0 ~ 2563.4m);ND-LITH (2072.6 ~ 2590.8m);GR-CORR (1825.0 ~ 2165.0m);COLLAR (2470.0 ~ 2515.0m)
102/16-06-045-04W5/00	SONIC (284.4 ~ 2597.2m);DIL (286.2 ~ 2595.7m);ND-LITH (2036.1 ~ 2597.2m);SONIC (2499.4 ~ 2946.2m);DIL (2499.4 ~ 2945.0m)
100/07-08-045-04W5/00	SONIC (270.7 ~ 2562.8m);NEUT (1219.2 ~ 2564.6m);LL (270.7 ~ 2564.0m);DEN (1219.2 ~ 2564.6m);CP (2447.5 ~ 2464.9m);CP (2011.7 ~ 2058.6m);CP (1798.3 ~ 1857.5m);CP (1210.1 ~ 1259.1m);CP (198.1 ~ 251.8m)
100/06-10-045-04W5/00	S (393.3 ~ 2505.8m);CNFD (393.3 ~ 2508.7m);DILL (393.3 ~ 2509.1m);GR-CB (164.0 ~ 2114.0m);COLLAR (2025.0 ~ 2115.0m)
100/14-09-045-05W5/00	ML (511.0 ~ 3056.0m);CS (511.0 ~ 3041.0m);CN-LD (511.0 ~ 3056.0m);DIL (511.0 ~ 3058.0m);TEMPL (749.0 ~ 1401.1m);GR-CB (1994.0 ~ 2171.0m);COLLAR (1998.0 ~ 2168.0m);CP (2142.0 ~ 2639.0m)

UWI	Wireline Geophysical Logs
100/04-22-045-05W5/00	IE (214.9 ~ 1341.7m);ML (1182.6 ~ 1339.6m);NEUT (30.5 ~ 3158.3m);IE (1341.7 ~ 1670.9m);ML (1339.6 ~ 1670.0m);NEUT (1158.2 ~ 1325.0m);IE (1670.9 ~ 2388.4m);ML (1182.6 ~ 2387.2m);IE (2388.4 ~ 3159.3m);ML (2387.2 ~ 3158.3m)
100/10-36-045-05W5/00	DIL (250.9 ~ 2514.6m);ND-LITH (579.1 ~ 2514.6m);CP (359.7 ~ 1926.9m);CP (1702.0 ~ 1772.7m);CP (1325.9 ~ 1379.5m);CP (1039.4 ~ 1098.5m);CP (155.4 ~ 192.0m)
100/01-01-046-01W5/00	SONIC (240.0 ~ 2253.0m);DIL (240.0 ~ 2255.0m);CB (1500.0 ~ 2256.3m);PERF (2195.0 ~ 2255.6m);COMP (2191.2 ~ 2252.3m);COLLAR (2192.0 ~ 2248.0m);DIR (240.0 ~ 2224.0m);CI (~ 232.0m);ND-LITH (240.0 ~ 2255.0m);COLLAR (2197.0 ~ 2244.0m)
100/02-01-046-01W5/00	CS (970.0 ~ 2283.2m);CNFD (246.0 ~ 2283.0m);DISF (246.0 ~ 2283.2m);C-VOL (246.0 ~ 2283.0m);COLLAR (2192.9 ~ 2256.0m);COLLAR (2204.0 ~ 2249.0m)
100/09-01-046-01W5/00	IE (234.1 ~ 2266.8m);SONIC (234.1 ~ 2265.3m);DIR (234.1 ~ 2266.8m);DIP (234.1 ~ 2266.8m)
104/06-06-046-01W5/00	CS (346.0 ~ 2170.2m);CN-LD (346.0 ~ 2178.7m);DIL (346.0 ~ 2181.7m);C-VOL (346.0 ~ 2178.7m);CS (2194.0 ~ 2470.5m);CN-LD (2194.0 ~ 2479.0m);DIL (2194.0 ~ 2482.0m);C-VOL (2194.0 ~ 2479.0m)
100/01-13-046-01W5/00	ES (194.5 ~ 2283.0m)
100/06-29-046-01W5/00	CS (395.0 ~ 983.0m);CNFD (395.0 ~ 992.0m);DISF (395.0 ~ 983.0m);GR-CB (1650.0 ~ 1750.0m);COLLAR (1693.0 ~ 1755.0m);CLITH (625.0 ~ 981.0m);CP (2285.0 ~ 2356.0m);CS (750.0 ~ 2448.0m);CNFD (750.0 ~ 2448.0m);CN-LD (750.0 ~ 2448.0m);DISF (750.0 ~ 2458.0m);COLLAR (1645.0 ~ 1683.0m);COLLAR (875.0 ~ 940.0m);COLLAR (875.0 ~ 910.0m);COLLAR (1570.0 ~ 1700.0m);COLLAR (874.0 ~ 1685.0m)
100/10-09-046-02W5/00	IE (1767.8 ~ 2790.7m);SONIC (284.4 ~ 1833.1m);DIL (204.8 ~ 1830.9m);PERF (1783.1 ~ 1840.1m);SONIC (1767.8 ~ 2789.8m)
100/10-25-046-02W5/00	IE (278.3 ~ 2690.2m);SONIC (278.3 ~ 2690.2m)
102/12-25-046-02W5/00	CS (884.0 ~ 2531.6m);CN-LD (1550.0 ~ 1800.0m);DIL (342.0 ~ 2543.1m);GR-CORR (1670.1 ~ 1749.2m);CP (1875.0 ~ 2545.0m);MUD-HYD (1550.0 ~ 2545.0m);GR-CORR (900.0 ~ 1774.0m)
100/11-12-046-03W5/00	ES (199.6 ~ 2560.0m);ML (609.6 ~ 2316.5m)
100/16-12-046-03W5/00	ES (171.6 ~ 2703.3m)
100/11-33-046-03W5/00	ES (180.7 ~ 2564.9m)
100/05-12-046-05W5/00	SONIC (458.7 ~ 2481.0m);DIL (17.7 ~ 459.3m);CI (~ 454.2m);ND-LITH (17.7 ~ 461.5m);DIL (458.7 ~ 2481.0m);ND-LITH (458.9 ~ 2481.0m)
100/06-19-046-05W5/00	IE (182.0 ~ 2863.3m);ML (899.2 ~ 2223.2m);MLL (2223.2 ~ 2864.5m)
100/10-20-046-05W5/00	SONIC (258.0 ~ 2563.0m);DIL (259.0 ~ 2562.0m);ND-LITH (1740.0 ~ 2563.5m)
100/14-29-046-05W5/00	S (400.0 ~ 2499.6m);CNFD (400.0 ~ 2494.3m);DIL (400.0 ~ 2508.5m)
100/09-10-047-01W5/00	ML (422.0 ~ 2077.0m);CS (2767.0 ~ 3101.0m);CN-LD (430.0 ~ 2070.0m);DISF (2769.0 ~ 3113.0m);DIRS (149.0 ~ 3115.0m);DIP (1775.0 ~ 2770.0m);CS (382.0 ~ 2076.0m);DISF (382.0 ~ 2076.0m);DIRS (10.0 ~ 2770.0m)
100/10-22-047-01W5/00	IE (242.3 ~ 2423.8m);SONIC (755.9 ~ 2423.8m);DIP (2057.4 ~ 2421.9m)
100/08-26-047-01W5/00	SONIC (247.5 ~ 2361.9m);DIL (247.5 ~ 2360.7m)
100/12-27-047-01W5/00	IE (245.7 ~ 2401.5m);SONIC (518.2 ~ 2401.2m);DIL (245.7 ~ 1006.8m);DEN (518.2 ~ 1007.1m);PERF (609.6 ~ 903.1m);FT (723.6 ~ 723.6m);FAL (1005.8 ~ 2399.1m)
100/16-35-047-01W5/00	SONIC (247.5 ~ 2290.9m);DIL (247.5 ~ 2290.0m);DEN (548.6 ~ 1981.2m)
100/06-02-047-02W5/00	IE (253.3 ~ 2514.6m);ML (253.3 ~ 2515.5m);SONIC (944.9 ~ 2513.7m);NEUT (1859.3 ~ 1950.7m);CAL (~ 1984.2m);FT (1718.8 ~ 1719.4m)
100/04-36-047-03W5/00	ES (185.9 ~ 2561.8m)
100/02-06-047-04W5/00	ES (203.0 ~ 3092.2m);ML (1051.6 ~ 3092.2m)

UWI	Wireline Geophysical Logs
100/09-24-047-06W5/00	CS (2246.1 ~ 2709.3m);CN-LD (2246.1 ~ 2709.3m);DISF (382.6 ~ 2247.8m);CP (2200.0 ~ 2724.0m);CS (382.6 ~ 2236.3m);CN-LD (800.0 ~ 2249.9m);DISF (2236.1 ~ 2720.5m)
100/16-02-048-01W5/00	ES (182.3 ~ 2286.0m)
100/02-21-048-01W5/00	IE (231.6 ~ 2286.0m);ML (231.6 ~ 2286.0m);SONIC (231.6 ~ 2284.8m);GR (1493.5 ~ 1573.4m);PERF (1521.0 ~ 1574.0m)
100/08-17-048-02W5/00	S (371.3 ~ 2046.2m);CNFD (1399.8 ~ 2048.8m);DILL (371.3 ~ 2049.8m);DIRS (397.0 ~ 2050.0m);DIP (1717.6 ~ 2053.5m);CP (300.0 ~ 1579.0m)
100/02-28-048-02W5/00	ES (190.5 ~ 2348.2m);ML (457.2 ~ 1188.7m);NEUT (61.0 ~ 2347.6m);CAL (579.1 ~ 1585.0m)
100/06-15-048-03W5/00	ES (1740.7 ~ 2672.5m);ML (823.0 ~ 1740.4m);NEUT (1859.3 ~ 2671.3m);DEN (~ 1737.4m);FT (1515.8 ~ 1515.8m)
100/16-06-048-04W5/00	IE (184.1 ~ 2873.0m);ML (670.6 ~ 2873.7m);SONIC (184.1 ~ 2872.1m)
100/08-15-048-04W5/00	ES (185.9 ~ 2559.7m);ML (701.0 ~ 1955.6m);NEUT (1554.5 ~ 2559.7m);MLL (1950.7 ~ 2237.2m);TEMP (304.8 ~ 1595.6m);CAL (701.0 ~ 1862.3m);GR-CORR (900.0 ~ 1335.0m)
100/10-29-048-05W5/00	SONIC (20.0 ~ 2215.6m);DIL (458.0 ~ 2218.0m);CB (800.0 ~ 2204.0m);GR-CB (950.0 ~ 1038.0m);GR (800.0 ~ 2204.0m);GR (975.0 ~ 1041.7m);ND-LITH (458.0 ~ 2217.6m);SONIC (2170.0 ~ 2350.0m);DIL (2217.5 ~ 2352.0m);ND-LITH (240.0 ~ 2351.0m)
102/14-12-048-06W5/00	S (384.8 ~ 2039.8m);CNFD (384.8 ~ 2039.0m);DISF (1450.0 ~ 2039.8m);GR-CB (100.0 ~ 1159.0m);GR-CORR (1000.0 ~ 1125.0m);DIP (2075.0 ~ 2414.0m);CP (2062.0 ~ 2414.0m);S (2039.0 ~ 2407.8m);CNFD (2039.0 ~ 2504.5m);DISF (2039.0 ~ 2413.7m);GR-CORR (1060.0 ~ 1115.0m)
100/14-29-048-06W5/00	ES (186.2 ~ 3115.4m);ML (853.4 ~ 3063.2m);NEUT (30.5 ~ 3145.8m);GRN-COL (795.0 ~ 1112.0m);GR-CORR (810.0 ~ 867.0m);COLLAR (325.0 ~ 350.0m)
100/04-11-049-01W5/00	ES (178.0 ~ 2128.7m)
100/16-33-049-01W5/00	ES (180.7 ~ 1491.7m)
100/15-11-049-02W5/00	ES (186.8 ~ 2262.5m)
100/07-33-049-06W5/00	IE (240.8 ~ 2322.6m);IEL (240.8 ~ 2329.0m);GRN-CB (1495.0 ~ 1835.2m);CNFD (241.0 ~ 2329.0m);TEMPL (15.0 ~ 1100.0m);GR-CB (1495.0 ~ 1835.2m);GR (1694.0 ~ 1836.0m);COLLAR (1728.0 ~ 1834.9m);ND-LITH (241.1 ~ 2322.6m);CP (290.0 ~ 1945.0m);COLLAR (290.0 ~ 331.0m);COLLAR (840.0 ~ 905.0m)
100/16-01-050-01W5/00	ES (189.9 ~ 2083.6m)
100/15-26-050-01W5/00	ES (185.9 ~ 1981.2m)
100/15-10-050-02W5/00	ES (77.7 ~ 2040.3m)
100/16-16-050-02W5/00	IE (223.4 ~ 2292.7m);ML (548.6 ~ 1583.1m);SONIC (1524.0 ~ 2291.2m);COMP (10.0 ~ 80.0m)
100/04-20-050-02W5/00	IE (236.5 ~ 1940.1m);ML (457.2 ~ 1941.9m);NEUT (15.2 ~ 1942.2m);COLLAR (10.0 ~ 90.0m);NEUT (1249.7 ~ 1562.4m);COLLAR (10.0 ~ 48.0m)
100/05-20-050-02W5/00	IE (228.6 ~ 2246.1m);SONIC (1310.6 ~ 2245.8m);DIP (1295.4 ~ 2243.6m);MS (1615.4 ~ 1950.7m)
100/10-21-050-02W5/00	ML (1260.0 ~ 1552.4m);ML-EL (402.0 ~ 1558.2m);CS (402.0 ~ 1555.8m);CNFD (402.0 ~ 1568.7m);DIL (402.0 ~ 1567.9m);ML-EL (1590.0 ~ 1887.8m);CS (1557.2 ~ 1884.5m);CNFD (1557.2 ~ 1898.1m);DIL (1557.2 ~ 1896.9m)
100/02-22-050-02W5/00	ES (184.7 ~ 1483.2m);ML (502.9 ~ 1289.9m);TEMP (182.9 ~ 843.4m);CAL (182.9 ~ 812.6m);GR (30.5 ~ 1081.1m);DIR (27.4 ~ 1084.8m)
100/02-26-050-02W5/00	ES (190.2 ~ 2243.3m);ML (426.7 ~ 1481.3m);CAL (190.2 ~ 1481.3m)
100/04-11-051-01W5/00	ES (185.9 ~ 2040.9m)
100/09-16-051-01W5/00	ES (190.2 ~ 2087.3m);ML (1341.1 ~ 1522.5m);NEUT (1417.3 ~ 1470.1m);COLLAR (273.3 ~ 1429.7m)
100/04-36-051-01W5/00	NLR

UWI	Wireline Geophysical Logs
100/04-28-051-02W5/00	ES (184.7 ~ 2182.4m)
100/04-14-051-03W5/00	IE (200.3 ~ 1905.0m);SONIC (200.3 ~ 1888.8m)
100/05-08-051-04W5/00	ML (229.8 ~ 1933.7m);DIL (229.5 ~ 1931.8m);ND-LITH (229.5 ~ 1933.0m);DIL (1889.8 ~ 2073.6m);ND-LITH (1889.8 ~ 2074.5m)
100/04-14-051-04W5/00	SONIC (235.9 ~ 1936.7m);DIL (235.9 ~ 1936.7m);DIP (1524.0 ~ 1889.8m);ND-LITH (1295.4 ~ 1937.3m);CP (1463.0 ~ 1516.1m);SONIC (1889.8 ~ 2057.4m);DIL (1889.8 ~ 2056.8m);ND-LITH (1889.8 ~ 2057.4m);CP (1036.3 ~ 1073.5m);CP (152.4 ~ 190.8m)
100/01-34-051-04W5/00	ML (231.0 ~ 2060.0m);DIL (231.0 ~ 2060.0m);COLLAR (10.0 ~ 132.0m);ND-LITH (200.0 ~ 1831.0m);CP (1734.0 ~ 1786.0m);CP (1300.0 ~ 1340.0m);CP (585.0 ~ 643.5m);CP (150.0 ~ 189.5m)
100/02-29-051-05W5/00	CS (360.0 ~ 2028.0m);CN-LD (360.0 ~ 2039.0m);DISF (360.0 ~ 2037.3m);TEMPL (10.0 ~ 1153.1m);CB-VD (300.0 ~ 660.0m);GR-CORR (1996.7 ~ 2030.3m);COLLAR (2008.2 ~ 2032.9m);CAS-COL (2008.2 ~ 2032.9m);CS (2041.0 ~ 2120.5m);CN-LD (2041.0 ~ 2115.0m);DISF (2041.0 ~ 2122.0m);CAS-COL (1030.5 ~ 1153.1m)
100/03-12-052-01W5/00	DIL (352.0 ~ 2072.0m);ND-LITH (352.0 ~ 2063.0m);CLOOK (1150.0 ~ 1525.0m);CP (1225.0 ~ 1300.0m);CP (250.0 ~ 302.0m)
100/09-13-052-01W5/00	ES (183.8 ~ 1830.0m)
100/10-05-052-02W5/00	IE (291.4 ~ 2918.8m);ML (291.4 ~ 2919.4m);SONIC (291.4 ~ 2919.4m)
100/04-34-052-03W5/00	ES (183.8 ~ 2103.1m)
100/11-34-052-03W5/00	CNFD (260.0 ~ 1808.5m);DIL (260.0 ~ 1808.5m);CP (375.0 ~ 1500.0m);CP (230.0 ~ 1815.0m)
100/15-23-052-04W5/00	SONIC (347.5 ~ 1945.7m);DIL (347.5 ~ 1954.5m);DIR (361.8 ~ 1930.9m);MS (1450.0 ~ 1508.6m);ND-LITH (347.5 ~ 1954.0m)
100/05-01-052-05W5/00	SONIC (214.6 ~ 2132.4m);DIL (214.6 ~ 2131.2m);DEN (1524.0 ~ 2132.4m);GR (1127.8 ~ 1269.2m)
100/16-18-052-05W5/00	ES (9.1 ~ 2797.1m);ML (670.6 ~ 1691.6m);ML (1630.7 ~ 2773.7m)
100/08-30-052-05W5/00	CS (426.3 ~ 2700.8m);CNFD (1190.0 ~ 1680.0m);DISF (426.3 ~ 2713.8m);DIF-CNS (8.0 ~ 426.5m);CAL (8.0 ~ 426.5m);CS (426.3 ~ 2700.8m);CNFD (1190.0 ~ 1680.0m);DISF (426.3 ~ 2713.8m);CLOOK (1400.0 ~ 1680.0m);CP (1600.0 ~ 2007.0m)
100/04-31-052-05W5/00	ML (462.0 ~ 1946.7m);SONIC (462.0 ~ 1946.0m);NEUT (1400.0 ~ 1700.0m);CNFD (462.0 ~ 1046.6m);DISF (462.0 ~ 1945.5m);CB (1400.0 ~ 1700.0m);PERF (1550.0 ~ 1625.0m);COLLAR (27.0 ~ 70.0m);ML (1946.5 ~ 2088.5m);CS (1946.5 ~ 2088.5m);CNFD (1964.5 ~ 2088.5m);DISF (141.0 ~ 2087.5m)
100/07-11-053-01W5/00	ES (186.8 ~ 1965.4m)
100/04-12-053-02W5/00	ES (184.7 ~ 1981.2m)
100/10-10-053-03W5/00	SONIC (190.5 ~ 1956.5m);DIL (190.5 ~ 1955.3m);ND-LITH (1341.1 ~ 1956.5m)
100/10-14-053-03W5/00	SONIC (196.9 ~ 1871.5m);NEUT (196.9 ~ 1873.3m);LL (196.9 ~ 1873.6m);DEN (196.9 ~ 1873.3m);CP (1554.5 ~ 1697.7m);CP (1249.7 ~ 1310.6m);CP (624.8 ~ 669.3m);CP (91.4 ~ 157.9m)
100/07-33-053-03W5/00	IE (184.1 ~ 1867.8m);ML (640.1 ~ 1768.8m);SONIC (184.1 ~ 1865.4m);FT (1513.6 ~ 1514.9m)
100/13-36-053-03W5/00	SONIC (201.4 ~ 1852.0m);DIL (201.4 ~ 1853.2m);ND-LITH (600.0 ~ 1852.8m);CP (486.2 ~ 500.8m);CP (388.6 ~ 406.0m);CP (342.9 ~ 358.5m);CP (175.3 ~ 191.1m);CP (45.7 ~ 54.6m)
100/13-36-053-05W5/00	ES (187.1 ~ 2067.2m)
100/03-16-043-05W5/00	(SCH, Rm=0.370@190F); ES (184.7 ~ 2073.2m); ML (1280.2 ~ 2072.0m); NEUT (15.2 ~3080.3m); ES (2073.2 ~ 3080.3m); ML (2164.1 ~ 3080.3m)
100/11-24-045-08W5/00	(DRA, Rm=0.280@95C); SONIC (456.0 ~ 3150.0m); DIL (456.0 ~ 3150.0m); CI (~442.0m); IND-LOG (30.5 ~ 481.6m); ND-LITH (456.0 ~ 3150.0m)
Table Legend	**Formation abbreviations**

UWI	Wireline Geophysical Logs
Blue Wells out of WASP study area Yellow Wells in Moon Lake play	List of log abbreviations available in WASP project archives.

APPENDIX 4: DRILL STEM TESTS

Recorded Measurements

(Source: Hydro-Fax Resources Ltd.)

Well Location	DST #	Test Date	Core?	BH Temp (°C)	BH Temp Source	Salinity (ppm)	Hydrofax Quality Assess.	Hydrofax Rated Perm	Recovery (m)
100/02-21-048-01W5/00	6	02/05/62		74.4	DST	125000	B	High	1136.9
100/04-20-050-02W5/00	4	12/18/58		51.1	DST	125000	D	High	1356.4
100/05-12-046-05W5/00	2	06/15/78	Y	70	Est.	135000	B	Average	128.1
100/06-05-045-04W5/00	4	02/16/75		77.8	DST	200000	A	Really High	951.1
100/07-08-045-04W5/00	3	03/15/76	Y	62.8	DST	200000	A	High	1756
100/10-05-052-02W5/00	3	12/19/67		56.7	DST	135000	A	Excellent	1310.7
100/10-09-046-02W5/00	4	01/17/66		72.2	DST	135000	B	Really High	320
100/10-14-053-03W5/00	4	01/20/76		70	Est.	135000	B	Really High	1355.4
100/10-20-046-05W5/00	6	11/04/78		70	Est.	135000	F	Low	1719
100/10-25-046-02W5/00	3	07/17/66		60	DST	135000	A	High	1498.7
100/10-27-044-03W5/00	7	11/30/77		76.7	DST	150000	B	High	1962.9
100/10-29-048-05W5/00	5	07/16/79		70	Est.	135000	A	High	1300
100/10-33-044-04W5/00	1	04/08/75		70	Est.	200000	A	High	1770.9
100/10-33-044-04W5/00	3	04/11/75		70	Est.	200000	A	Really High	417.6
100/13-36-053-03W5/00	1	07/06/78	Y	42	DST	135000	A	Excellent	1267
100/14-21-045-02W5/00	2	08/19/60		82.2	DST	135000	B	High	1585
100/14-21-045-02W5/00	3	08/28/60		70	DST	135000	D	High	521.2
100/14-29-046-05W5/00	2	06/27/93		95	DST	135000	F	Low	114
100/15-35-044-02W5/00	2	02/03/88		71.3	DST	135000	C	Average	367
102/14-12-048-06W5/00	3	04/05/89		77.7	DST	135000	A	Excellent	1690
102/16-06-045-04W5/00	1	07/27/75		80.6	DST	200000	A	Really High	541.6
102/16-06-045-04W5/00	3	08/09/75		87.8	DST	200000	A	Really High	823

Hydrofax Ratings

Code	Quality Status	Permeability
A	Very good test	High to Excellent
B	Good test	Average to Relatively High
C	Fair test	Relatively Low to Average
D	OK test	Relatively Poor
E	Poor	Tight
F	Very poor test	Very Low to Low
G	Recovery data only	No reliable data

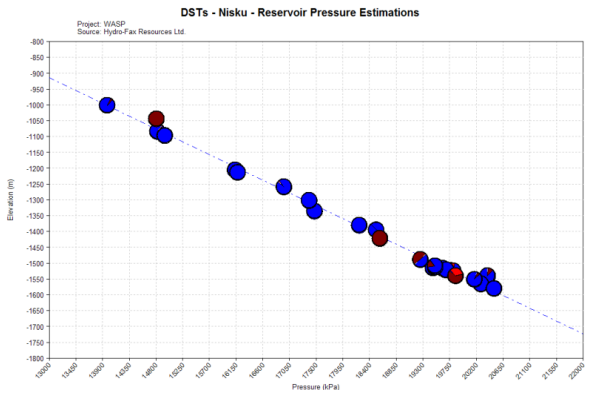

WASP Project DST Analysis

Well Location	k (mD)	kh (mD.m)	s*	p* (kPa)	m (kPa/ cycle)	Quality Assess.	Reason	Form.	Interval (m KB)	
100/02-21-048-01W5/00	39.201	203.84	-4.696	14908		Poor	Stair-stepping	Dnisku	1878.5	1883.7
100/04-20-050-02W5/00	10.041	1.53E+02	-4.524	15054		Poor		Dnisku	1854.7	1869.9
100/05-12-046-05W5/00	0.011	0.33	-0.247	19094		Mediocre		Dnisku	2383.5	2414
100/06-05-045-04W5/00	1.078	16.39	-0.822	19798	6086.87	Poor	PPD erratic	Dnisku	2519.5	2534.7
100/07-08-045-04W5/00	19.264	292.82	-4.286	19661		Poor	Stair-stepping	Dnisku	2507	2522.2
100/10-05-052-02W5/00	N/A	N/A	N/A	14054		Poor	No resolution	Dnisku	1740.4	1758.7
100/10-09-046-02W5/00	9.335	98.96	30.925	16883	411.42	Mediocre	Pressure Low	Dnisku	2220.5	2231.1
100/10-14-053-03W5/00	0.671	3.09	-3.957	15329		Mediocre	Pressure Low	Dnisku	1780	1784.6
100/10-20-046-05W5/00	3.45	68.99	-3.485	20208		Poor	PPD erratic	Dnisku	2460	2480
100/10-25-046-02W5/00	N/A	N/A	N/A	N/A		Poor	No resolution	Dnisku	2121.4	2129
100/10-27-044-03W5/00	1.122	34.57	-3.337	18487		Poor	PPD erratic	Dnisku	2339.6	2370.4
100/10-29-048-05W5/00	N/A	N/A	N/A	18337		Poor	No resolution	Dnisku	2215.9	2236
100/10-33-044-04W5/00	2.818	68.47	-3.379	19676		Poor	Too Few Points	Dnisku	2511.6	2535.9
100/10-33-044-04W5/00	0.349		-2.108	21646		Poor	Low resolution	Dnisku	2510.6	2514.3
100/13-36-053-03W5/00	14.107	98.75	-5.334	14086		Poor	Stair-stepping / Low Pressure	Dnisku	1759	1766
100/14-21-045-02W5/00	74.125	719.01	-4.96	17559		Poor	Poor resolution	Dnisku	2246.4	2256.1
100/14-21-045-02W5/00	0.328	5.81	0.391	17335		Poor	Poor resolution	Dnisku	2216.2	2233.9
100/14-29-046-05W5/00	0.003	0.03	-0.645	7282		Poor	Pressure Low / Temp High	Dnisku	2470	2480
100/15-35-044-02W5/00	0.011	0.39	-1.037	17111		Mediocre		Dnisku	2185	2219
102/14-12-048-06W5/00	N/A	N/A	N/A	18972		Poor	No resolution	Dnisku	2300	2335
102/16-06-045-04W5/00	0.865	15.83	-1.456	19896		Interm.	2nd slope used for p*	Dnisku	2525.3	2543.6
102/16-06-045-04W5/00	0.89	13.08	-1.304	19702		Poor	Low resolution	Dnisku	2522.5	2537.2

Notes

1. Quality assessment based on number and distribution of recorded values for estimation of reservoir pressure and permeability using Horner plot analysis method.
2. DST data available in WASP project archives.

APPENDIX 5: FORMATION WATER RESISTIVITY

UWI	Resistivity	Resistivity Temp	Rw @ 70 °C	log Rw	Well Name
100/02-28-048-02W5/00	0.1	25	0.0508	-1.2940	TEXACO SOCONY WARBURG A-2-28
100/02-28-048-02W5/00	0.1	25	0.0508	-1.2940	TEXACO SOCONY WARBURG A-2-28
100/04-20-050-02W5/00	0.07	25	0.0356	-1.4489	TEXACO TELFORDVILLE 4-20-50-2
100/05-20-050-02W5/00	0.09	72	0.0920	-1.0364	MIDWEST TELFORDVILLE 5-20-50-2
100/05-20-050-02W5/00	0.06	72	0.0613	-1.2125	MIDWEST TELFORDVILLE 5-20-50-2
100/10-05-052-02W5/00	0.08	20	0.0363	-1.4403	HOME CPOG BRIGHTBANK 10-5-52-2
100/10-14-053-03W5/00	0.07	25	0.0356	-1.4489	AMOCO B-2 WABAMUN LAKE 10-14-53-3
100/07-33-053-03W5/00	0.08	20	0.0363	-1.4403	M.W. GAS WABAMUN 7-33-53-3
100/07-33-053-03W5/00	0.08	20	0.0363	-1.4403	M.W. GAS WABAMUN 7-33-53-3
100/13-36-053-03W5/00	0.06	25	0.0305	-1.5158	HOME ALBERTA BEACH 13-36-53-3
1F1/11-29-045-02W5/00	0.056	25	0.0285	-1.5458	KETCH RES WROSES 11-29-45-2
		Median =	0.0363	-1.4403	
		Average =	0.0449	-1.3743	

UWI	Date Sampled	Depth Interval (m)		Na	Ca	Mg	Cl	Bicarb	Sulfate	TDS (calc)
100/02-28-048-02W5/00	01/05/1955	1956.8	2026.9	45309	11089		88830	500	500	146228
100/02-28-048-02W5/00	01/04/1955	1956.8	1964.1	27378	8332		56272	550	500	93032
100/04-20-050-02W5/00	12/18/1958	1854.7	1870.0		16930		118419	317	377	
100/05-20-050-02W5/00	10/10/1965	1847.4	1853.5	24953	3376	1152	46581	1037	840	77939
100/05-20-050-02W5/00	10/02/1965	1847.4	1853.5	44047	9688	1934	89689	813	720	146891
100/10-05-052-02W5/00	12/29/1967	1740.4	1758.7	47218	10250	2255	96600	600	785	157708
100/10-14-053-03W5/00	01/20/1976	1780.0	1784.6	46138	11340	1417	95014	513	24	154446
100/07-33-053-03W5/00	10/17/1961	1581.6	1589.5	43493	7928	2168	86850	366	487	141292
100/07-33-053-03W5/00	10/22/1961	1746.5	1751.1	41102	8834	2168	83955	497	1481	138037
100/13-36-053-03W5/00	07/05/1978	1759.0	1766.0	45018	10890	2193	94200	361	942	153604

Source: GeoFluids database at IHS Energy and well-file information for 1F1/11-29-045-02W5/00. For more complete water chemistry information, see the geochemistry portion of the full report.

APPENDIX 6: POROSITY AND PERMEABILITY (INBOARD PLATFORM MARGIN)

Based on a conceptual understanding of the depositional setting for Nisku carbonates within the WASP study boundary (Figure 1 in text) and direct evidence (core observations) outside the study area, it is thought that the inboard margin of the upper Nisku should include zones of enhanced porosity and permeability. The inboard edge marks the eastern boundary of marine-based deposition for the Nisku and is a transitional zone into evaporate/hypersaline facies of the Nisku abundant to the southeast of the study area (Figure 1). More intense wave action and generally energetic conditions favourable for reef growth were thought to have been present during the upper Devonian along this inboard edge (Figure 1 and Figure 3 in text for reference). As there are limited direct observations via core, the next best option is an analysis of existing wireline data specifically comparing wells that are thought to be located along this edge versus wells which are well away from this edge.

Our assessment of the sonic data (see graph below) suggests:

The sonic transit times along the inboard edge are NOT necessarily better for targeting enhanced porosity zones in the open marine facies relative to the entire population of wells. For the hypersaline facies location is irrelevant to log response.

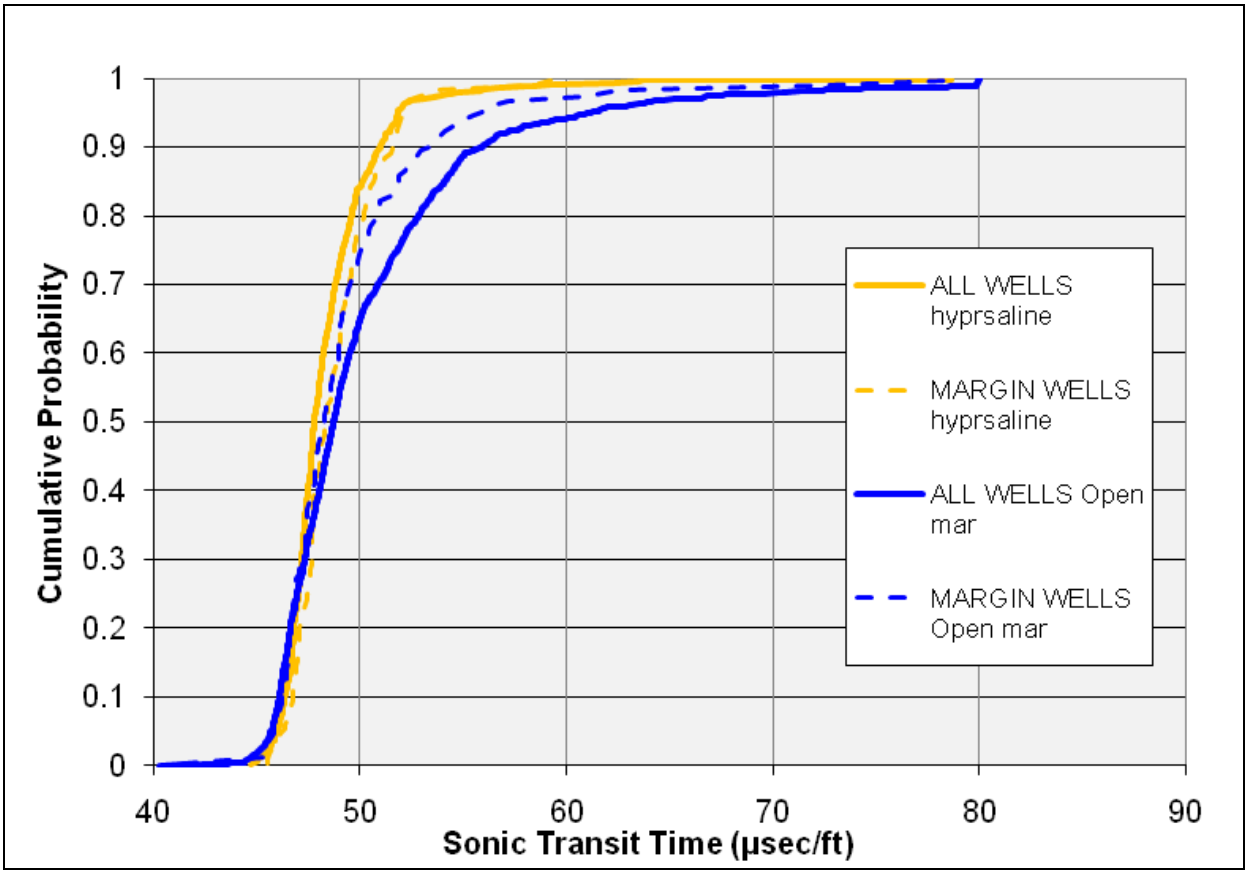

For resistivity log data the interpretation is the same (see plot below; upper set of curves uses the top and right axes; lower set of curves uses lower and left axes).